MR Imaging of Benign and Malignant Biliary Conditions

James R. Costello, MD, PhD[a,b], Bobby Kalb, MD[a,b,*], Surya Chundru, MD[a,b], Hina Arif, MD[a,b], Iva Petkovska, MD[a,b], Diego R. Martin, MD, PhD, FRCPC[a,b]

KEYWORDS

• MRCP • MR imaging • Bile ducts • Choledocholithiasis • Primary sclerosing cholangitis • Cholangiocarcinoma • Posthepatic transplant evaluation • Hepatobiliary-specific contrast agents

KEY POINTS

- MR imaging is a noninvasive, radiation-free imaging method for evaluation of the biliary system. Continued advancements in MR imaging system hardware and sequence design, coupled with novel gadolinium chelate agents, allow for a detailed evaluation of the bile ducts and surrounding soft tissues.
- The full diagnostic potential of MR imaging is achieved by coupling the luminal evaluation of fluid-sensitive MR cholangiopancreatography (MRCP) sequences with the soft tissue assessment of dynamic, contrast-enhanced three-dimensional T1-weighted (T1W) gradient echo (GRE) sequences and shorter echo, single-shot T2-weighted (T2W) sequences.
- The capability for soft tissue assessment is a specific strength of MR imaging over luminal-only imaging techniques, such as endoscopic retrograde cholangiopancreatography (ERCP).
- Choledocholithiasis is the most common cause for bile duct obstruction and is well-depicted on MRCP sequences, whereas associated inflammatory changes in the bile duct wall and hepatic parenchyma are demonstrated on sequences highlighting soft tissue detail.
- New hepatocyte-specific contrast agents may hold utility in the anatomic and functional evaluation of bile duct injury. MR imaging is also the imaging method of choice for bile duct tumor diagnosis, staging, and presurgical planning.
- Familiarity with the proper methodology of MR image acquisition and interpretation is critical for optimized diagnostic assessment.

INTRODUCTION

The biliary system may be afflicted by a wide range of benign and malignant pathology, and is a major source of morbidity and mortality in the United States. A variety of disease processes affecting the bile ducts may have similar clinical presentations, and medical imaging plays a central role in the diagnosis and treatment decision pathways for these patients. Although ultrasound and computed tomography are frequently used modalities for imaging of biliary disease (especially in the

Disclosures: None.

[a] Department of Medical Imaging, University of Arizona, 1501 North Campbell Avenue, PO Box 245067, Tucson, AZ 85725, USA; [b] Body Division, Department of Medical Imaging, University of Arizona, 1501 North Campbell Avenue, PO Box 245067, Tucson, AZ 85725, USA

* Corresponding author. Body Division, Department of Medical Imaging, University of Arizona, 1501 North Campbell Avenue, PO Box 245067, Tucson, AZ 85725.

E-mail address: bkalb@radiology.arizona.edu

Magn Reson Imaging Clin N Am 22 (2014) 467–488

http://dx.doi.org/10.1016/j.mric.2014.05.002

1064-9689/14/$ – see front matter

emergency setting), the soft tissue capabilities of MR imaging are ideally suited for providing a comprehensive analysis of bile duct pathology. With continued advancements in hardware innovation and sequence design, coupled with new gadolinium-based chelate agents that are excreted by the biliary system, MR imaging continues to assume a central role in the diagnostic work-up of bile duct diseases. This article describes standard and newly developed MR imaging methods for imaging the biliary tree. An array of benign and malignant biliary pathology is presented, with concentration on the MR imaging features and specifics of optimized image interpretation.

MR IMAGING METHODOLOGY

MR Cholangiopancreatography

MR cholangiopancreatography (MRCP) is the key MR imaging sequence for luminal imaging of the biliary tree. By using a heavily T2-weighted (T2W) sequence with echo times in excess of 700 milliseconds, MRCP provides excellent anatomic detail of the fluid-containing structures of the abdomen, and is ideally suited for imaging of the bile ducts. Several different technical approaches to MRCP may be pursued. Conventional two-dimensional MRCP sequences constitute the fastest and most frequently used method. Single-shot, turbo spin echo sequences (obtained through the application of a single 90-degree pulse followed by an echo train of multiple 180-degree pulses with separate phase-encoding gradients) are resistant to patient motion and produce reliable image quality even in sick and freely breathing patients. Two-dimensional MRCP images may be acquired as either a thick-section coronal slab image and/or thin, multisection stacked images. The coronal slab MRCP is typically a 5- to 6-cm thick section that may be acquired in a short breath hold of 5 seconds, providing a single image overview of the biliary and pancreatic ductal systems. A potential limitation of the thick slab technique is the possibility of partial volume averaging effects that may obscure small filling defects within the biliary tree. This limitation may be overcome by the additional acquisition of contiguous, axial multisection MRCP images through the biliary tree. When acquired with a single-shot technique, this sequence is quite resistant to patient motion and may better demonstrate small calculi in the biliary system.[1–3]

Three-dimensional acquisition MRCP methods are also available that produce high-quality, isotropic resolution images of the biliary system. Using a three-dimensional T2W turbo-spin echo method with echo times in excess of 700 milliseconds, a volumetric data set may be produced with 1-mm thin sections and no intersection gaps or image misregistration effects. Postprocessing of this raw, volumetric data may be performed with multiplanar reconstruction to produce thin section data in multiple imaging planes, in addition to maximum intensity projections with volume rendering to produce a rotating, overview image of the biliary system. Image acquisition times for the three-dimensional technique are variable, although they are typically on the order of 4 to 8 minutes. Respiratory triggering is a necessary component of this sequence because of the longer image acquisition time. Triggering methods vary, but a common technique tracks diaphragmatic motion in real time to trigger image acquisition at specific points in the respiratory cycle. Variability of the respiratory cycle and the ability of each breath to meet the set trigger thresholds are factors that directly influence the time of image acquisition.[4]

The criteria for selection of a three- or two-dimensional MRCP technique may vary from center to center (**Fig. 1**). Three-dimensional acquisition methods offer the strengths of excellent contrast and improved signal-to-noise ratios relative to the two-dimensional techniques. In addition, the high-resolution method of a three-dimensional acquisition allows for more reliable distinction of small biliary calculi from flow artifacts than may be seen with the two-dimensional method. However, the larger time investment required for three-dimensional image acquisition may discourage some centers from routine use of this technique. Additional soft tissue imaging obtained as part of a comprehensive MR examination of the bile ducts frequently provides additional diagnostic information that may reduce the benefits of the three-dimensional MRCP technique. In patients with irregular respiratory cycles that are difficult to capture by the navigator pulse, there may be a significant time investment in a three-dimensional image acquisition that is susceptible to ghosting and blurring artifacts. In comparison, two-dimensional methods tend to be much more robust and resistant to motion degradation.[4,5]

Preimaging patient instructions vary from center to center. A common imaging protocol instructs patients to fast for 4 hours before the MR imaging to reduce the amount of fluid in the stomach and duodenum, which may obscure visibility of the biliary system on MRCP sequences. Other centers routinely use negative oral contrast agents (eg, blueberry juice or iron oxide agents)[6] to reduce overlapping T2 signal in the stomach and proximal small bowel. However, the benefits of these preimaging instructions are reduced when soft tissue imaging becomes a standardized part of abdominal imaging protocols for bile duct imaging.

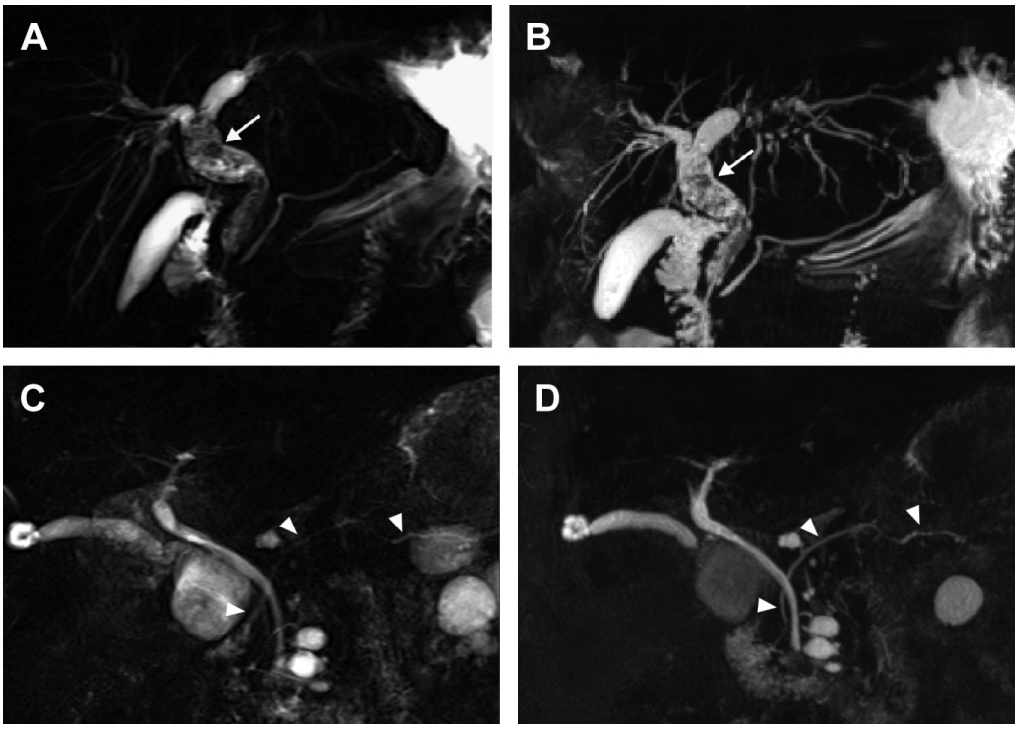

Fig. 1. Two- and three-dimensional MRCP. A 52-year-old woman with type IVa choledochal cyst depicted with two-dimensional (*A*) and three-dimensional (*B*) MRCP techniques. Note the dilated common bile duct (CBD) filled with stones (*arrows, A* and *B*) that are demonstrated on both techniques. The acquisition time for the three-dimensional technique in this patient was 5 minutes, whereas the acquisition time for the two-dimensional technique was 5 seconds. A 72-year-old man with intraductal papillary mucinous neoplasm (IPMN) undergoing both two-dimensional (*C*) and three-dimensional (*D*) MRCP. Note improved visualization of the pancreatic duct with the three-dimensional technique compared with the two-dimensional method (*arrowheads, C* and *D*).

Soft Tissue Imaging

Despite the many benefits of MRCP, obtaining this sequence alone is insufficient for a comprehensive analysis of the biliary system. MRCP is a luminal technique and does not provide adequate analysis of the surrounding soft tissues that are frequently a contributor to biliary pathology. It is our view that an imaging evaluation of the bile ducts is incomplete without dynamic, T1-weighted (T1W) contrast-enhanced three-dimensional gradient echo (GRE) sequences coupled with shorter echo, single-shot T2W sequences. MRCP is simply one additional component of a comprehensive MR imaging examination that has the ability not only to diagnose the presence of biliary obstruction, but also to provide a specific pathologic cause for the obstruction.

T2W and steady-state free precession imaging

Although MRCP sequences provide a luminal depiction of the biliary system, T2W sequences with shorter echo times (approximately 80–90 milliseconds at 1.5 T) combine the advantages of producing high signal in the biliary system with the ability to assess the surrounding soft tissues. When acquired with a single-shot technique, these sequences are motion insensitive and produce consistently high image quality. The T2W images are prone to through-plane flow artifacts, manifesting as foci of signal loss in fluid-containing structures. These flow artifacts are typically centrally located within the extrahepatic bile duct on axial images and are not present on coronal sequences. Steady-state free precession sequences, like T2W sequences, produce bright signal in fluid-containing structures. However, even when acquired with a single-shot technique, steady-state free precession sequences are less prone to this flow void artifact and may be helpful to distinguish between small stones and flow artifact in questionable cases (**Fig. 2**).[1,2]

T1W imaging

Dynamic, fat-saturated gadolinium chelate–enhanced T1W three-dimensional GRE imaging is a critical portion of a comprehensive MR imaging evaluation of the intrahepatic and extrahepatic bile ducts. This technique is performed during a single breath hold and is thus sensitive to motion artifact. Recently, newer T1W three-dimensional GRE sequences have been developed that use a radial pattern of k-space filling, reducing flip angle inaccuracies and motion artifacts and thus preserving image quality even in freely breathing patients.[7,8]

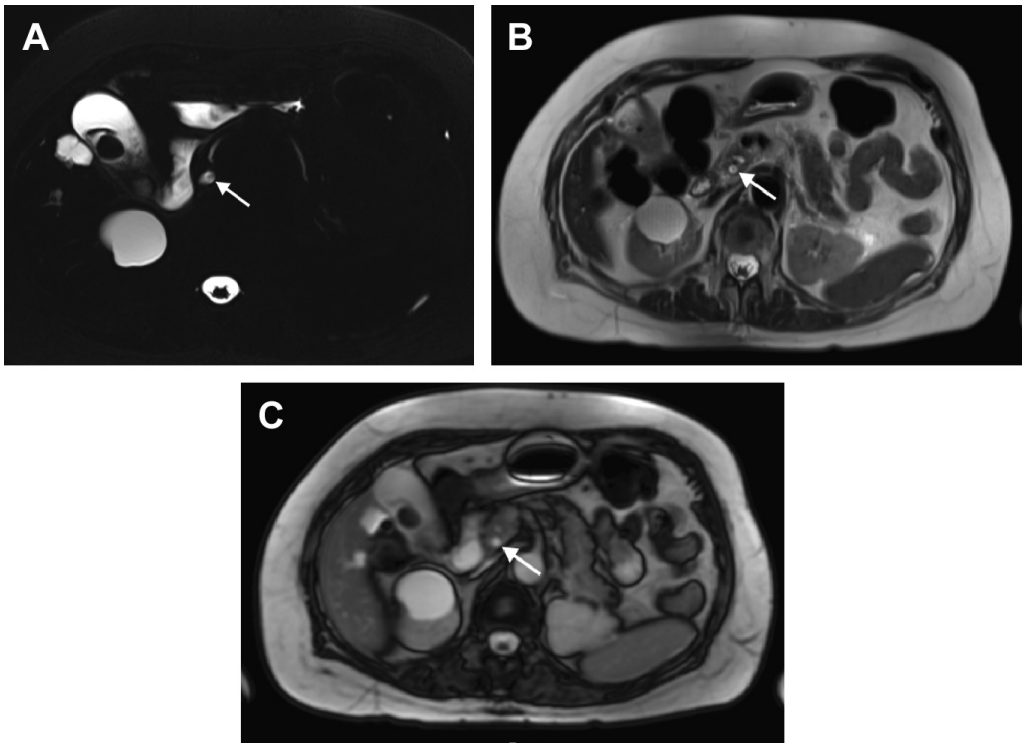

Fig. 2. A 43-year-old man with flow void artifact in the CBD. Axial single-shot MRCP (*A*) and T2W (*B*) images demonstrate a small hypointense focus (*arrow*) located centrally in the CBD, not layering along the dependent surface as would be expected with a bile duct stone. Steady-state free precession image (*C*) does not show the hypointense flow void artifact (*arrow*).

Precontrast T1W images are helpful in demonstrating blood products, cholesterol-laden stones, and sludge in the biliary system. In addition, interruption of bile flow by obstructive processes causes accumulation of bile acids in the hepatic parenchyma, inciting a hepatic inflammatory response and hepatocyte injury.[9] A dynamic, arterial-phase sequence acquired with a bolus tracking method frequently demonstrates these changes of active hepatitis.[10] These findings are typically only apparent on a properly timed arterial-phase acquisition, normalizing on subsequent venous and delayed interstitial phase images. In addition, infiltrative tumor growing along the duct wall and abnormal soft tissues causing extrinsic compression of the bile ducts may be reliably differentiated with dynamic postcontrast imaging.[11]

Hepatobiliary-Specific Contrast Agents

Although most gadolinium chelate agents have a primarily extracellular biodistribution with renal clearance, a few agents have come to market in recent years that have a mixture of renal and hepatic clearance. Gadoxetate disodium (Gd-EOB-DTPA; Eovist or Primovist, Bayer Healthcare, Leverkusen, Germany) is a liver-specific agent that is excreted 50% by the liver and 50% by the kidneys in patients with normal hepatic and renal function. This agent is transported from the extracellular space into the hepatocytes by an ATP-dependent transporter and subsequently excreted into the bile duct canaliculi,[12] shortening the T1 of fluid in the bile ducts and producing high signal on T1W sequences. Gd-EOB-DTPA is typically excreted into the biliary system by 7 to 10 minutes, with serial imaging usually obtained through 20 minutes postinjection. This feature of contrast excretion into the biliary system has allowed for new methods of bile duct imaging using high-resolution, isotropic T1W three-dimensional GRE sequences as an alternative to T2W three-dimensional MRCP. This technique finds promising application for preoperative planning and for assessment of bile duct injuries.[13] It should be noted that the optimum excretion of a hepatocyte-specific agent into the bile duct canaliculi depends on properly functioning hepatocytes. Inflamed liver tissue, whether related to intrinsic acute or chronic hepatitis or alternatively bile duct obstruction, may not take up and excrete the contrast into the biliary system in a reliable fashion. Gadobenate dimeglumine (Multihance; Bracco Diagnostics, Monroe Township, NJ, USA) is another contrast agent with hepatic uptake and excretion, producing signal in the biliary system after 1 to 2 hours postinjection, but to a much lesser extent than Gd- EOB-DTPA. Mangafodipir trisodium (Teslascan; Nycomed, Zurich,

Switzerland) is a paramagnetic manganese-based agent that also demonstrates some biliary excretion, but was recently withdrawn from the market because of low demand.

THE EVOLVING ROLE OF MR IMAGING AND ENDOSCOPIC RETROGRADE CHOLANGIOPANCREATOGRAPHY

Endoscopic retrograde cholangiopancreatography (ERCP) is a commonly used procedure for evaluation of the biliary tree. Advantages of ERCP include the ability to perform therapeutic interventions including cytologic brushings, stone extraction, and stent placement for obstructive diseases. As a diagnostic imaging modality, ERCP has several disadvantages compared with MR imaging. ERCP is an invasive methodology, and complications include postprocedure pancreatitis, bleeding, cholangitis, and perforation. A large, multicenter review found the overall ERCP complication rate to be 6.85%[14] and the ERCP-related mortality rate to be 0.33%, with some studies reporting 1%.[15] Performed by opacifying the biliary system with iodinated contrast, ERCP only provides a luminal evaluation of the bile ducts and frequently fails to visualize the biliary system proximal to a point of obstruction or high-grade narrowing. ERCP demonstrates even more limited application in the setting of biliary enteric anastomoses or other surgically altered anatomy. In the evaluation of malignant biliary disease, ERCP cannot assess for extraductal disease and is limited in tumor staging. By contrast, MR imaging is a noninvasive imaging technique with no radiation or need for sedation, and provides a comprehensive assessment of not only the lumen of the biliary system but also the surrounding soft tissues.

Several studies have demonstrated the ability of MR imaging to diagnose biliary diseases, with sensitivities and specificities greater than 90%, comparable with ERCP.[16–19] An optimal imaging strategy uses MR imaging as the initial diagnostic modality for the evaluation of the bile ducts. When intervention is required, the MR imaging findings may be used as a roadmap for subsequent endoscopic intervention. This approach results in overall cost savings for the medical system[15] in addition to reducing the number of patients exposed to procedural complications.[20]

BENIGN HEPATOBILIARY PATHOLOGY

Biliary Obstruction

Choledocholithiasis

Stones in the biliary tree are the most frequent cause of bile duct obstruction. MR imaging demonstrates sensitivity (81%–100%) and specificity (85%–100%) for the diagnosis of biliary stones that is comparable with ERCP and superior to computed tomography and ultrasound.[1] On T2W images, biliary calculi present as hypointense filling defects surrounded by bright fluid (**Fig. 3**). Stones as small as 2 mm are reliably identified in dilated and nondilated systems. Smaller calculi are best imaged with thin-section MRCP images and may be obscured by thick-section slab or maximum intensity projection reconstructions secondary to volume averaging.[1]

MR imaging aids in the diagnosis of Mirizzi syndrome, which occurs when a stone impacted within the cystic duct results in obstruction of the adjacent common hepatic duct (**Fig. 4**). MR imaging not only highlights the stone within the cystic duct but also details the surrounding inflammatory signal, allowing reliable differentiation from cholangiocarcinoma.[21]

When interpreting the biliary system on MR imaging, note should be made of several potential mimics that may resemble bile duct calculi. As previously noted, rapid flow of bile may produce a flow void artifact within the duct on single-shot T2W images, which may be misinterpreted as a calculus. Pneumobilia may also present as a filling defect in the biliary system, but is differentiated from a dependently layered calculus by its nondependent position within the biliary tree and/or the presence of an air-fluid level. In addition, air demonstrates “blooming” artifact on dual-GRE, in-phase images because of the effects of gas on the local magnetic field (**Fig. 5**). Blood clots may be difficult to differentiate from biliary calculi on T2W images, but on noncontrast T1W imaging they present with high signal intensity (**Fig. 6**).

Portal biliopathy

Portal biliopathy is a term used for obstruction of the bile ducts from extensive varices at the porta hepatis, typically a result of portal venous thrombus. Chronic occlusion of the portal vein leads to cavernous transformation with distention of several venous plexuses that extend along the biliary tree, and may cause bile duct obstruction through extrinsic compression. On MR imaging, portal biliopathy manifests as smooth narrowing and scalloping of the bile duct wall, which is compressed by the surrounding venous collaterals (**Fig. 7**). Although MRCP sequences depict the bile duct obstruction, the key to accurate diagnosis is identification of the extensive venous collaterals on soft tissue imaging, clearly detailed on dynamic contrast-enhanced T1W three-dimensional GRE imaging.[22,23]

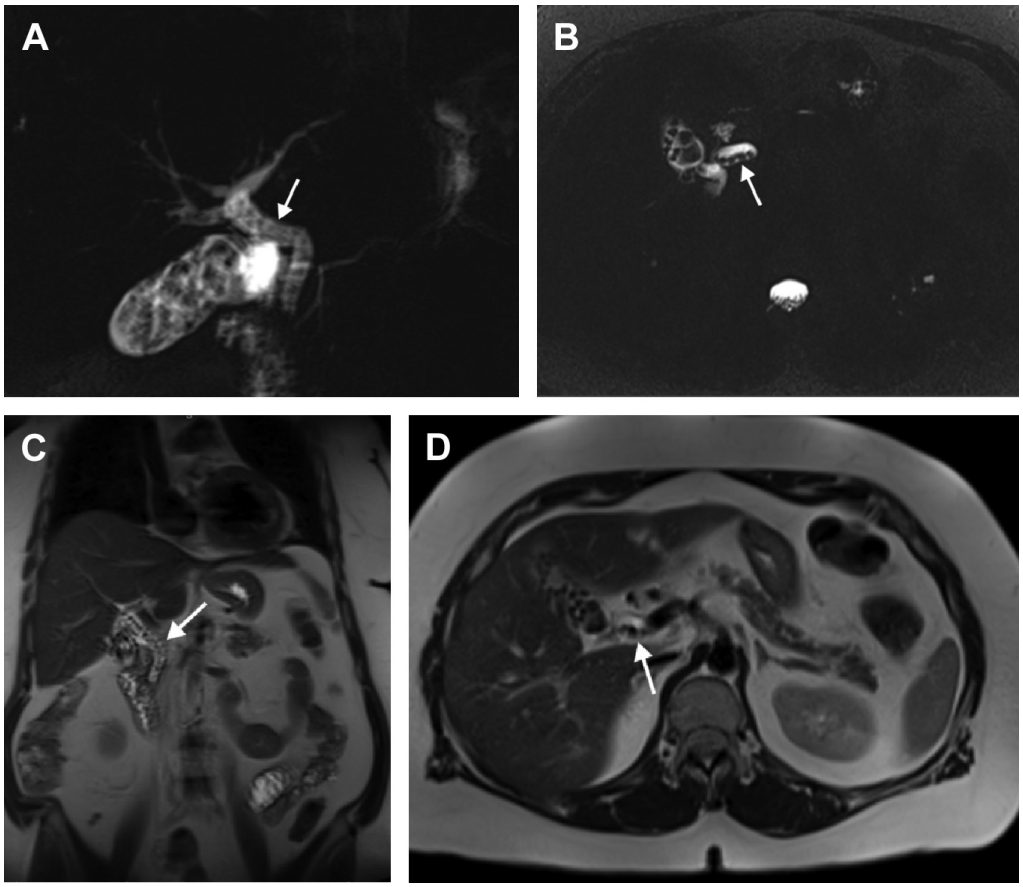

Fig. 3. A 56-year-old woman with abdominal pain and choledocholithiasis. Coronal slab (*A*) and axial single-shot (*B*) MRCP demonstrates multiple small stones filling the CBD (*arrows*, *A* and *B*) in addition to gallstones. The stones (*arrow*) are also well demonstrated on coronal (*C*) and axial (*D*) single-shot T2W images, which depict not only choledocholithiasis but also the surrounding soft tissues.

Cystic Disease of the Bile Ducts

Choledochal cysts are congenital cystic dilatations of the biliary tree, which were first classified by Alonso-Lej in 1959 and expanded to a five-category system by Todani in 1977 (Fig. 8). Choledochal cysts are distinguished from obstruction by the cystic morphology and the localized pattern of dilatation.[24,25]

There is an increased risk of carcinoma in choledochal cysts.[26] More than 90% of these congenital cysts are associated with an anomalous pancreaticobiliary junction, permitting reflux

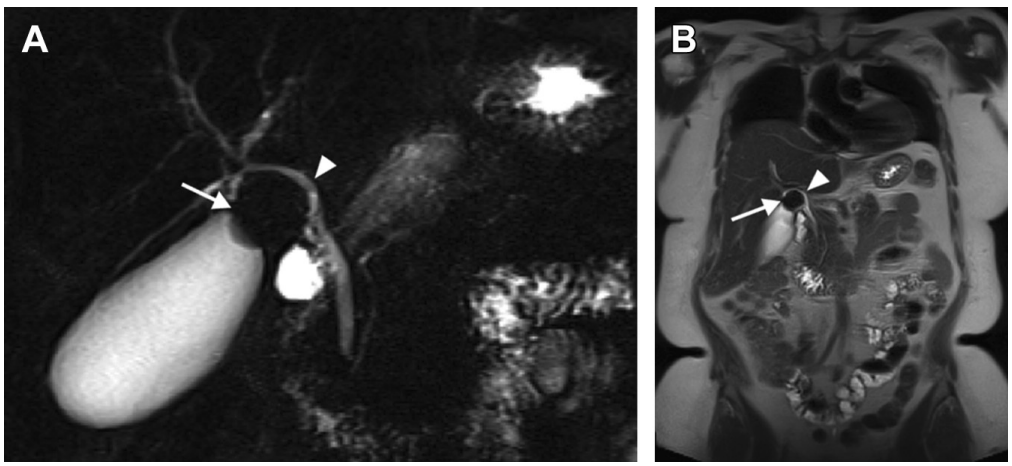

Fig. 4. A 57-year-old woman with Mirizzi syndrome. Coronal slab MRCP (*A*) and coronal single-shot T2W (*B*) images demonstrate a large stone lodged at the neck of the gallbladder (*arrows*, *A* and *B*). This stone is causing mass effect on the adjacent common hepatic duct (CHD) (*arrowheads*, *A* and *B*), resulting in mild obstruction of the intrahepatic bile ducts.

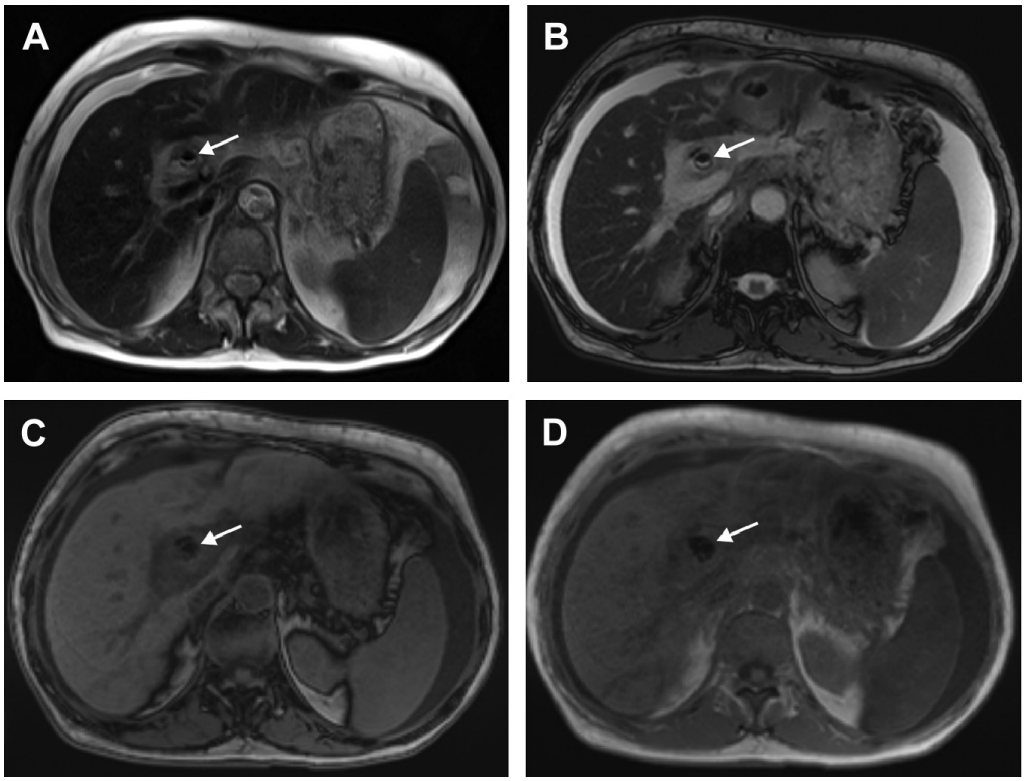

Fig. 5. A 62-year-old man with pneumobilia status post-ERCP. Axial single-shot T2W (*A*) and steady-state free precession (*B*) images show hypointense signal in the CHD (*arrows*, *A* and *B*). This signal layers nondependently with a meniscus appearance in keeping with an air-fluid level. Air in the biliary system is confirmed on dual echo T1W GRE sequences (out-of-phase *C* and in-phase *D*), which demonstrate "blooming" artifact of the gas on the longer echo, in-phase image (*arrows*, *C* and *D*).

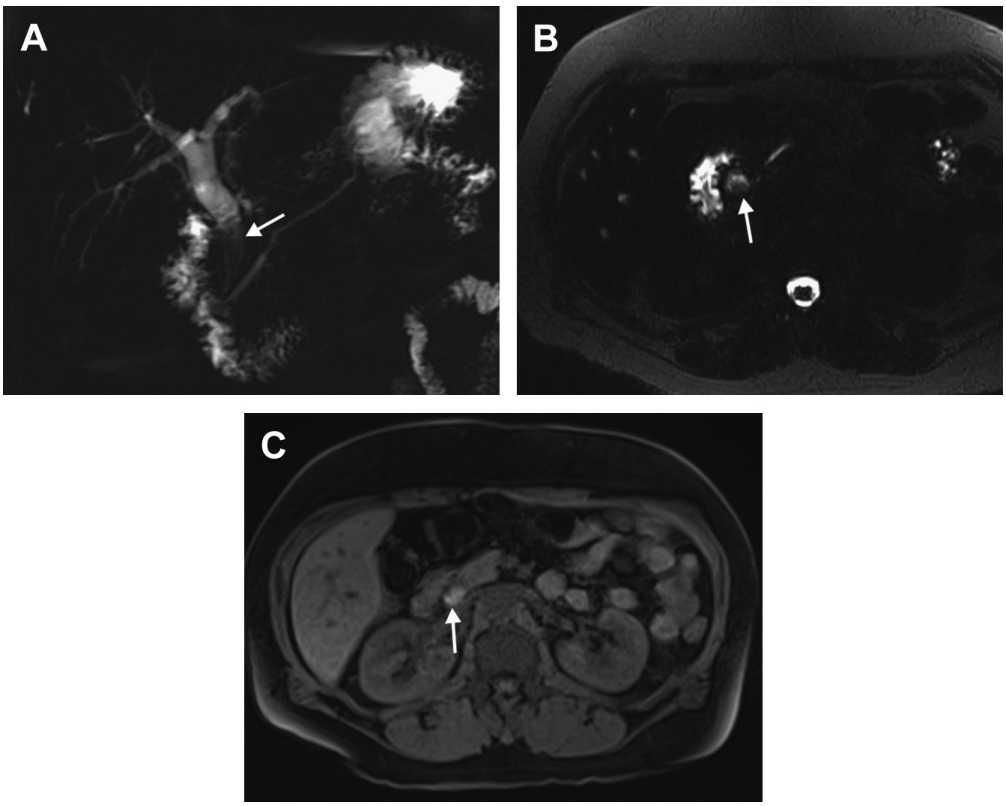

Fig. 6. A 39-year-old man with acute postprocedural pain following ERCP. Coronal slab (*A*) and axial single-shot (*B*) MRCP demonstrate a filling defect layering in the distal CBD (*arrows*, *A* and *B*), causing mild intrahepatic and extrahepatic bile duct dilatation. (*C*) Axial, fat-suppressed T1W three-dimensional GRE sequence (*arrow*) demonstrates elevated T1 signal in this material filling the distal CBD, suggestive of blood products given the recent procedure. The patient underwent repeat ERCP with extraction of a large clot.

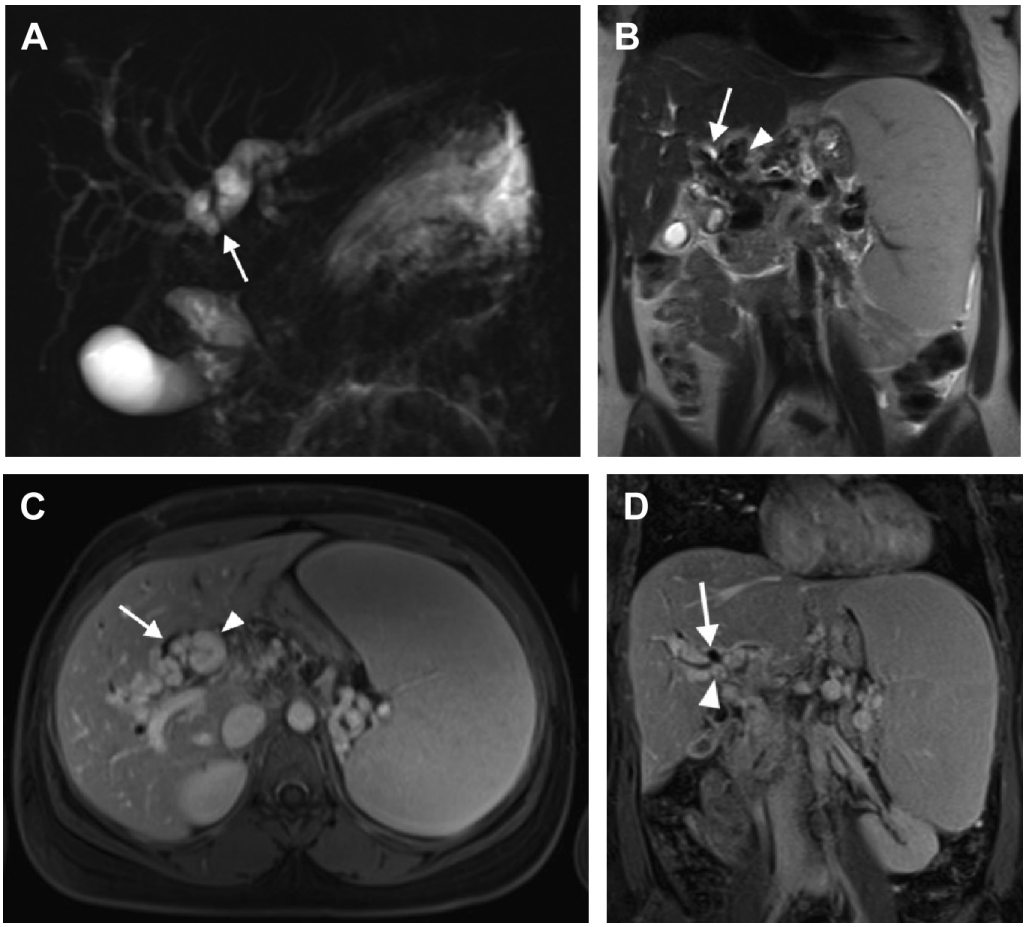

Fig. 7. A 59-year-old man with chronic liver disease and biliary obstruction. (*A*) Coronal slab MRCP demonstrates obstruction of the intrahepatic bile ducts at the level of the confluence (*arrow*). (*B*) Coronal ssT2 image depicts multiple, serpiginous T2-hypointense flow voids (*arrowhead*) surrounding the CHD (*arrow*) at the level of obstruction. Axial (*C*) and coronal (*D*) T1W three-dimensional GRE sequences demonstrate multiple venous collaterals (*arrowheads*, *C* and *D*) surrounding the biliary confluence (*arrows*, *C* and *D*). Note the added value of soft tissue imaging in this case, which clearly demonstrates the cause of biliary obstruction in this patient with cavernous transformation of the portal vein and portal biliopathy. Massive splenomegaly is also noted.

of pancreatic enzymes up into the biliary system and likely predisposing to cancer.[27] For this reason, many of these patients are treated with cyst resection and hepaticojejunostomy. These patients remain at increased risk for subsequent development of bile duct cancer throughout their lifetime.[28] MR imaging, using a combination of T2W sequences and dynamic, postcontrast T1W imaging, has the ability to assess the morphology of the choledochal cyst and also to screen for carcinoma by depicting coexistent enhancing soft tissue elements (**Fig. 9**).

Inflammatory Diseases of the Bile Ducts

Bile stasis

A stone in the extrahepatic bile duct frequently results in inflammatory changes of the hepatic parenchyma because of obstruction of bile flow from the liver into the gut. This stasis of bile in the liver incites an inflammatory response that is manifested clinically by a transient increase in hepatic enzymes. This hepatic inflammation is well demonstrated on MR imaging by a heterogeneous enhancement pattern of the liver on a properly timed, parenchymal arterial-phase sequence (**Fig. 10**).[29] In worsening hepatic inflammation, parenchymal T2 signal is also elevated because of fluid shifts and edema.

Infectious cholangitis

Ascending cholangitis results from partial or complete biliary obstruction with microorganisms traveling from the duodenum into the biliary tree. Acute cholangitis is demonstrated on MR imaging by periportal edema and distention of the biliary tree on T2W sequences. In addition, there is progressive enhancement of the bile duct wall on fat-suppressed, contrast-enhanced T1W sequences during the portal venous and delayed venous phases (**Fig. 11**).[30] Thrombosis of the right or left portal vein is a commonly associated finding.[31]

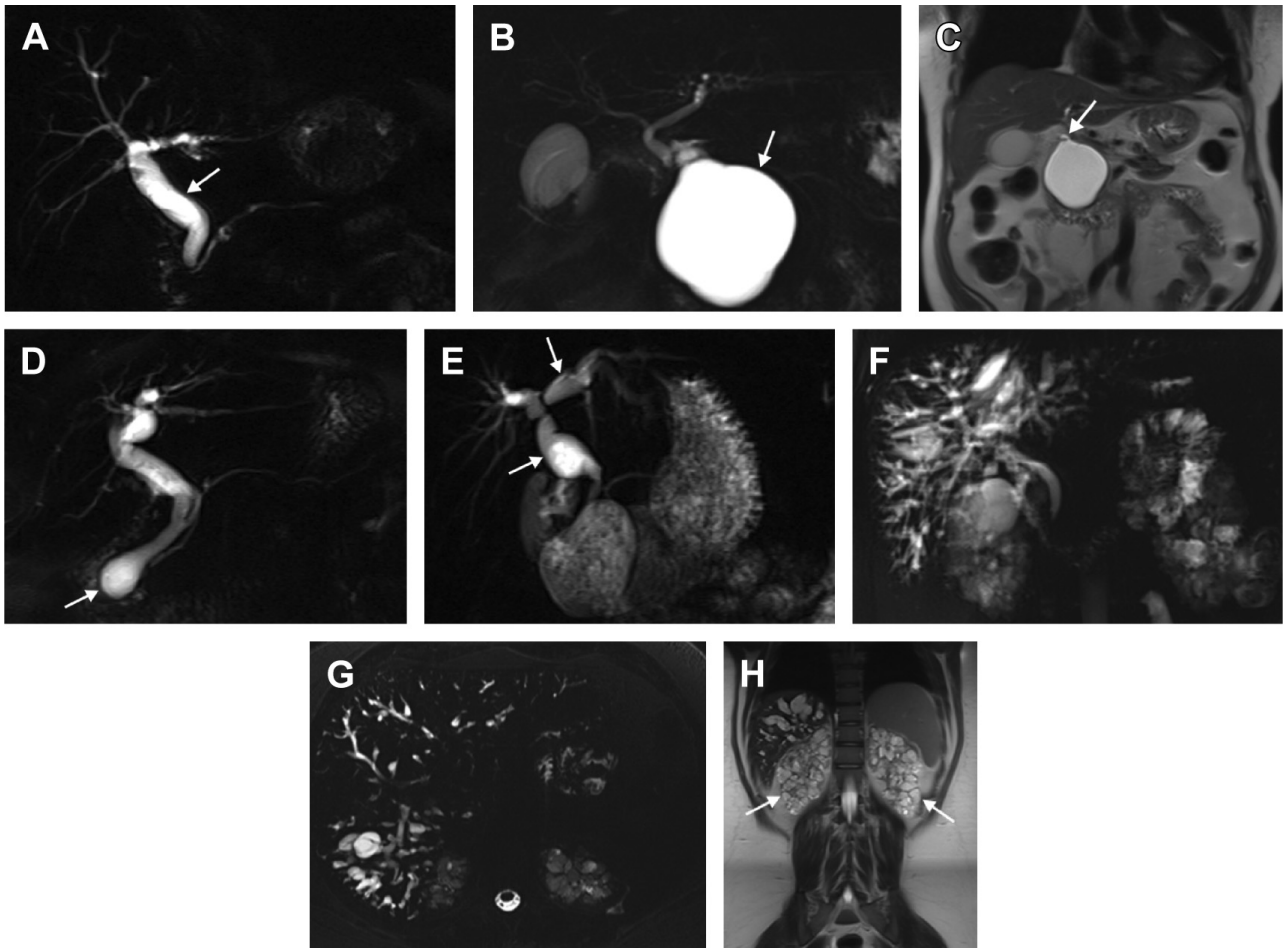

Fig. 8. Todani classification of choledochal cysts. (*A*) Type I choledochal cyst is characterized by diffuse, fusiform dilatation of the CBD (*arrow*) with relative sparing of the intrahepatic bile ducts. (*B*, *C*) Type II choledochal cyst presents as a diverticulum (*arrow*, *B*) arising from the extrahepatic bile duct with a small communication typically identified (*arrow*, *C*). (*D*) Type III choledochal cyst is also termed a choledochocele. In this type, there is more focal dilatation of the very distal CBD with prolapse into the ampulla (*arrow*). (*E*) Type IV choledochal cysts are subclassified into type IVa with multiple cystic dilatations of the intrahepatic and extrahepatic bile ducts (*arrows*) and also type IVb with multiple cystic dilatations involving only the extrahepatic bile ducts (not pictured). (*F–H*) Type V choledochal cyst is synonymous with Caroli disease, manifested by multiple, extensive cystic dilatations of the entire intrahepatic biliary system (*F* and *G*). Note that Caroli disease is frequently associated with autosomal-recessive polycystic kidney disease, which is also present in this pediatric patient (*arrows*, *H*).

Recurrent pyogenic cholangitis constitutes a particular type of infectious cholangitis caused by *Clonorchis sinensis* or other parasites. This infectious process results in periductal fibrosis with stricturing of the bile ducts, emergence of pigmented calculi, and evolution of periductal abscesses. On MR imaging, there is distention of the biliary tree proximal and distal to the calculi (**Fig. 12**). For recurrent pyogenic cholangitis, MRCP illustrates 100% of distended biliary ducts segments, 96% of focal strictures, and 98% of pigmented calculi.[32] The hepatic lobes that contain pigmented calculi within their biliary tree often develop lobar atrophy. Given the increased incidence for cholangiocarcinoma with recurrent pyogenic cholangitis, a thorough examination with dynamic, contrast-enhanced T1W imaging should be performed to exclude any associated neoplasm.[33]

Primary sclerosing cholangitis

Primary sclerosing cholangitis (PSC) represents an immune-mediated disease causing inflammation and fibrosis of the intrahepatic and extrahepatic biliary ducts with subsequent chronic cholestasis. This progressive disease process leads to multifocal, irregular stricturing of the bile ducts with interposed sections of ductal dilatation producing a "beaded" morphology. With involvement of the higher-order peripheral ducts, the biliary tree assumes a "pruned" appearance, defined as a 4-cm or longer segment of dilated duct that lacks the expected side branching. PSC is best diagnosed from the composite picture of a cholestatic biochemical profile, an exclusion of attributable secondary causes, and description of the standard morphologic bile duct changes[19] optimally depicted with MR imaging (**Fig. 13**).

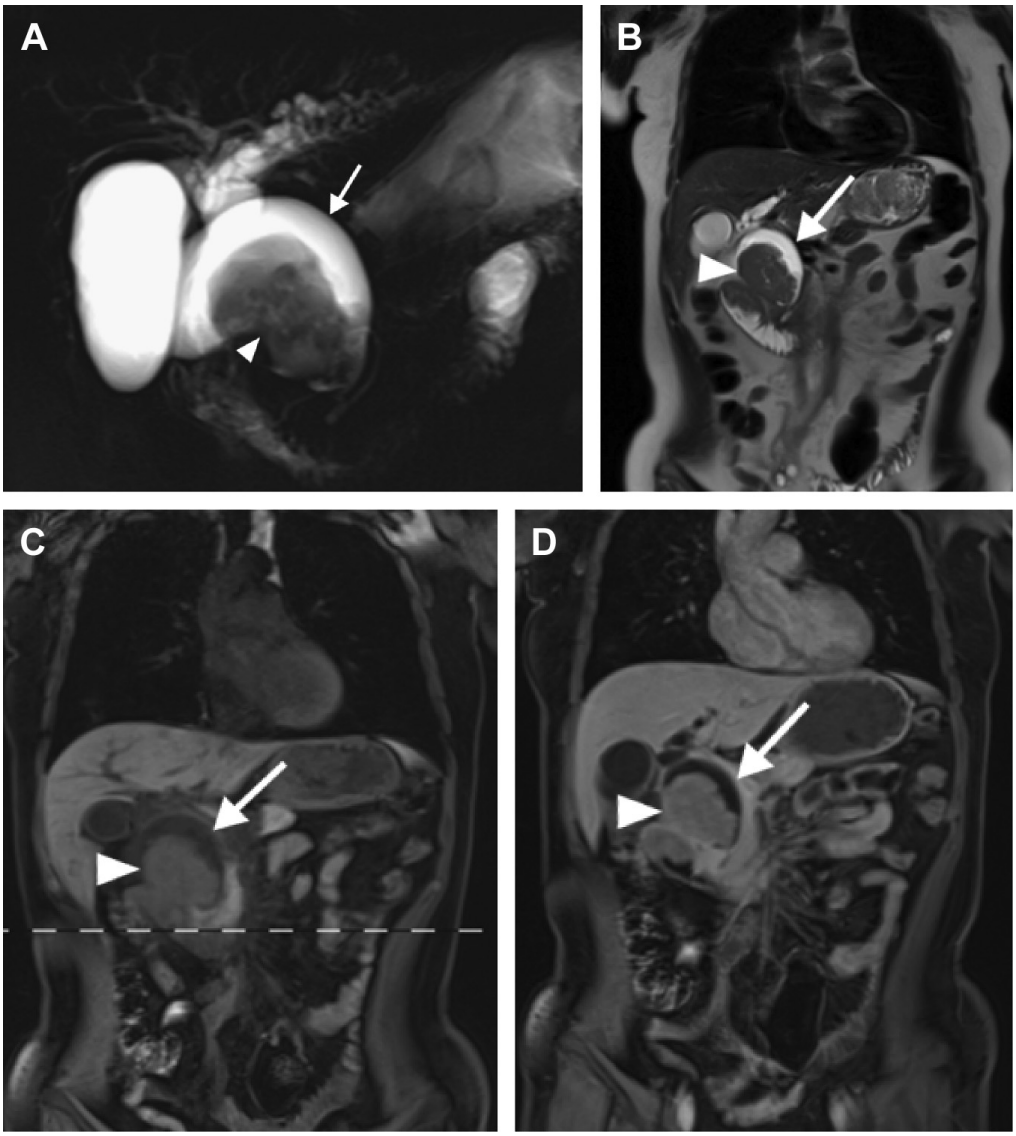

Fig. 9. A 35-year-old woman with cholangiocarcinoma arising in a choledochal cyst. Coronal slab MRCP (*A*) and coronal single-shot T2W (*B*) images demonstrate marked dilatation of the extrahepatic bile duct (*arrows*), which is filled with soft tissue along its lateral margin (*arrowheads*); the intrahepatic bile ducts are also dilated. Coronal precontrast (*C*) and postcontrast (*D*) T1W three-dimensional GRE sequences demonstrate heterogeneous enhancement (*arrowheads*) of this soft tissue filling the choledochal cyst (*arrows*). Surgical resection confirmed cholangiocarcinoma arising from a pre-existing type IVa choledochal cyst.

Patients with PSC are at increased risk for the development of cholangiocarcinoma, with a 10-year cumulative risk of cholangiocarcinoma of 7% to 9%. These patients require serial follow-up examinations, preferably with MR imaging, to assess for the development of any potentially malignant stricture. Cholangiocarcinoma occurs with greatest frequency in the perihilar region, and fat-suppressed, contrast-enhanced T1W sequences are critical to evaluate for any potential obstructing soft tissue (**Fig. 14**).[19,27,34]

IgG4-related sclerosing cholangitis

IgG4-related systemic sclerosing cholangitis is a fibroinflammatory disorder of multiple organ systems, which most commonly manifests with autoimmune pancreatitis. Extrapancreatic involvement of this disease involves the bile ducts in 68% to 88% of cases. On MR imaging, IgG4-related cholangitis demonstrates diffuse thickening of the biliary system (**Fig. 15**). In 35% of cases, there is a pattern of multiple biliary strictures that may mimic PSC.[35] Depending on the extent of bile duct wall thickening and fibroinflammatory change, this entity may be difficult to distinguish from carcinoma. The presence of coexistent autoimmune pancreatitis (best depicted with MR imaging) is often key to the diagnosis.

Acquired immunodeficiency cholangiopathy

In patients infected with HIV, inflammation of the bile duct mucosa results in an interrupted pattern of biliary strictures and segmental dilatations, resembling the “pruned” tree pattern of PSC.

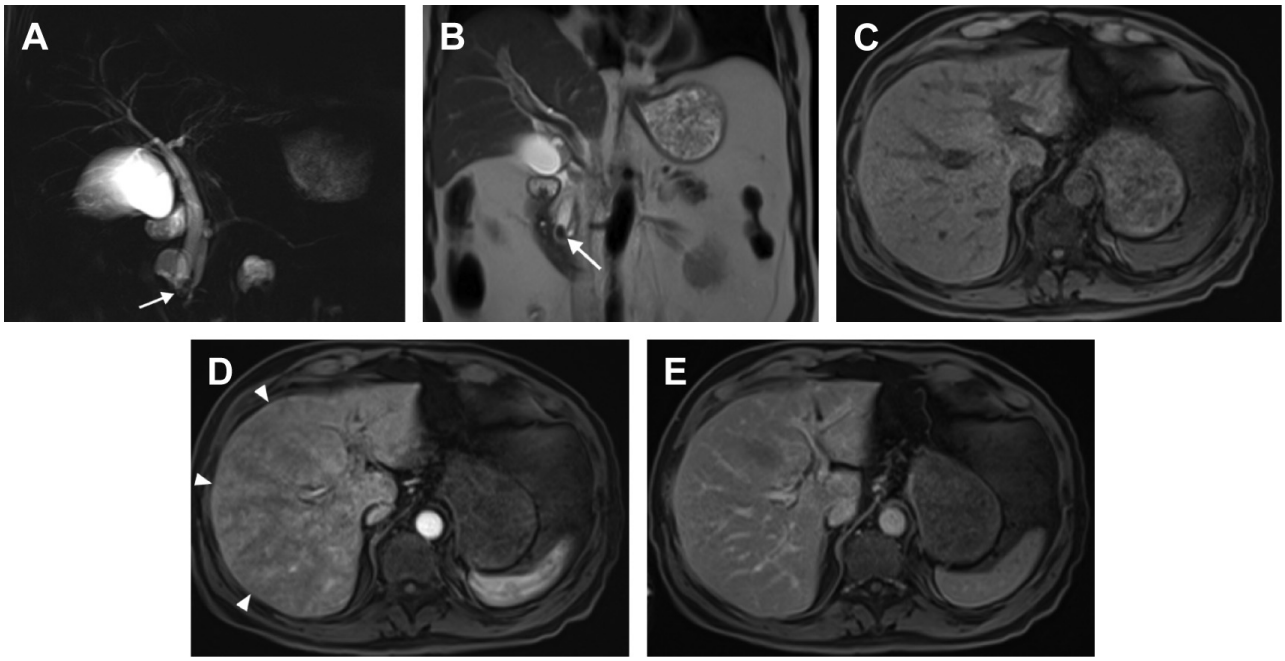

Fig. 10. A 47-year-old woman presents to the emergency room with acute right upper quadrant pain. Coronal slab (*A*) and coronal single-shot T2W (*B*) images demonstrate an obstructing stone lodged at the ampulla (*arrows*). Note the improved detection of the stone on the single-shot T2W images, secondary to overlying fluid partially obscuring this region on the MRCP slab in this acutely ill patient. Axial precontrast (*C*), arterial-phase (*D*), and delayed phase (*E*) images demonstrate marked heterogeneous enhancement of the hepatic parenchyma on arterial-phase images (*arrowheads*, *D*). Note that the heterogeneous enhancement normalizes on the delayed, interstitial phase sequence (*E*).

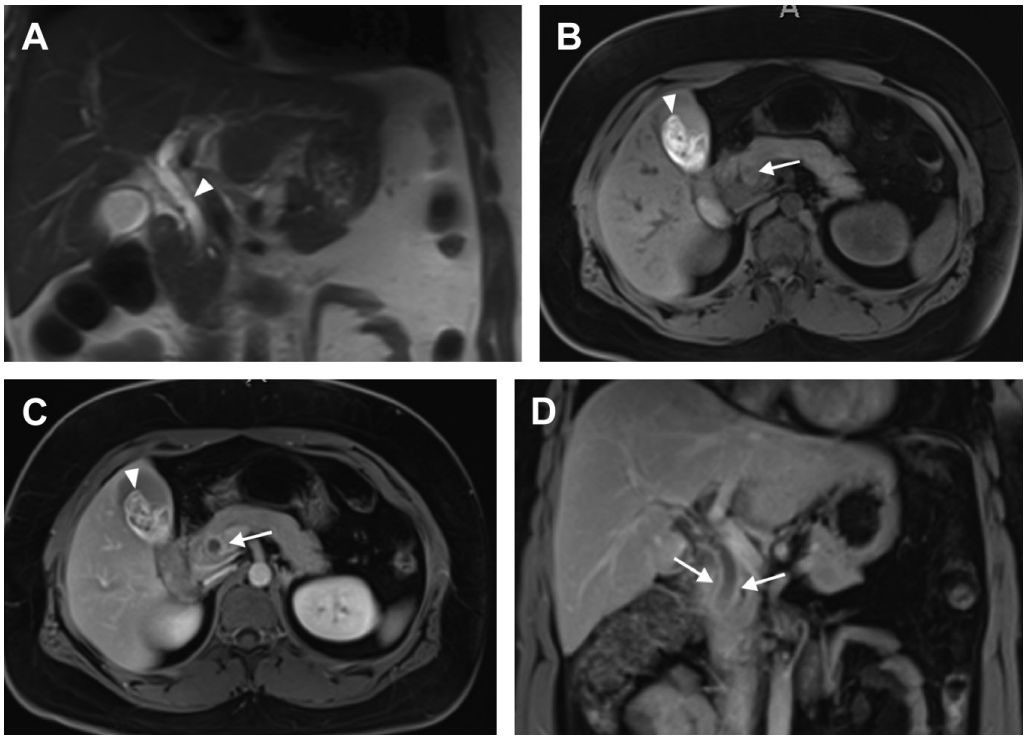

Fig. 11. A 37-year-old woman with right upper quadrant pain and fever. (*A*) Coronal single-shot T2W image demonstrates mild dilatation of the CBD (*arrowhead*). Axial precontrast (*B*), axial (*C*), and coronal (*D*) delayed-phase postcontrast T1W three-dimensional GRE sequences show marked thickening of the bile duct epithelium (*arrows*, *B–D*) in this patient with acute cholangitis. Findings were believed to be secondary to a recently passed stone, given the stones and sludge in the gallbladder (*arrowheads*, *B* and *C*). The patient recovered with antibiotic therapy and supportive measures.

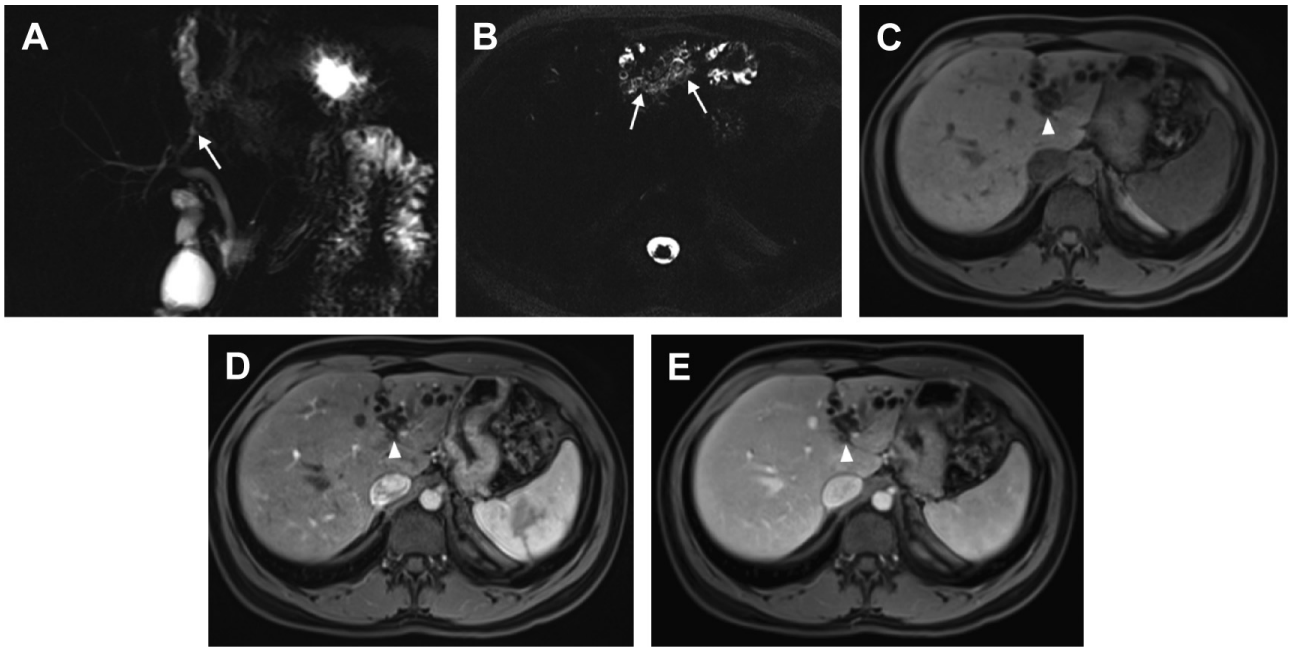

Fig. 12. A 42-year-old woman with recurrent pyogenic cholangitis. Coronal slab (*A*) and axial single-shot (*B*) MRCP demonstrate focally dilated, stone-filled bile ducts in the left hepatic lobe (*arrows*). Axial precontrast (*C*), arterial (*D*), and delayed-phase (*E*) T1W three-dimensional GRE sequences show no abnormal soft tissue at the site of stricture (*arrowheads*, *C–E*) to suggest an obstructing neoplasm.

Most patients suffering from AIDS cholangiopathy have a CD4 count less than 100/mm^3. AIDS cholangiopathy is classically distinguished from PSC by the presence of long segment strictures of the extrahepatic bile ducts. Frequently, there are associated findings of papillary stenosis; other associated findings include acalculous cholecystitis and ascending infectious cholangitis from such opportunistic infections as cytomegalovirus and *Cryptosporidium parvum*. AIDS cholangiopathy is also frequently associated with lymphoma, Kaposi sarcoma, and cholelithiasis.[36,37]

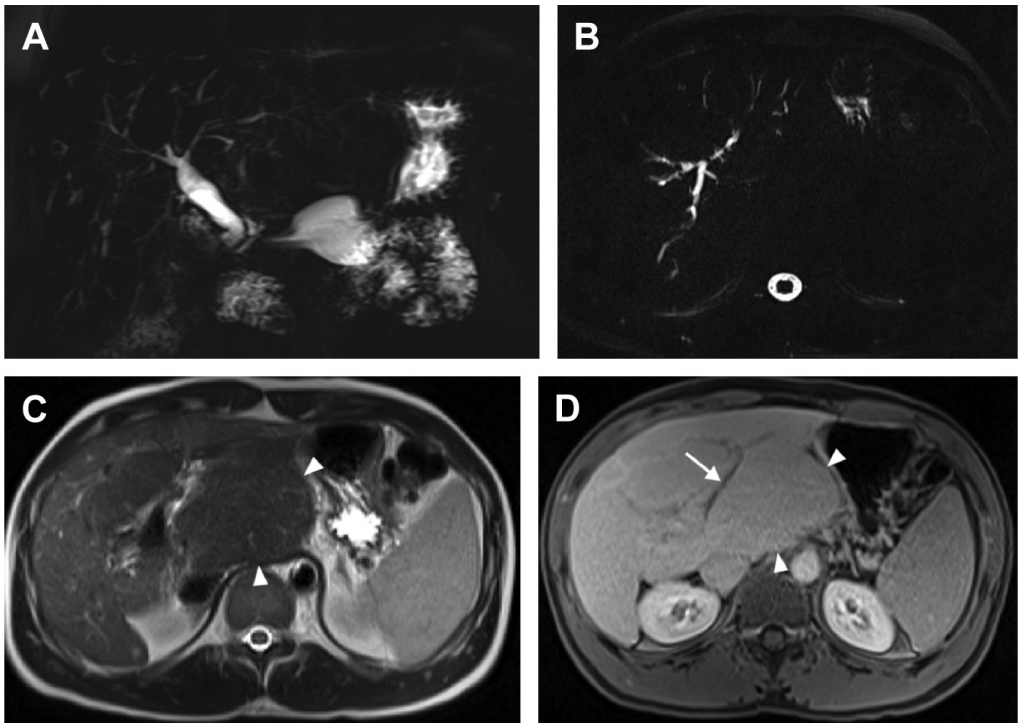

Fig. 13. A 49-year-old woman with PSC. Coronal slab (*A*) and axial single-shot (*B*) MRCP demonstrated a beaded appearance of the intrahepatic bile ducts with multifocal strictures. Axial single-shot T2W (*C*) and delayed post-contrast (*D*) images demonstrate the dilated intrahepatic bile ducts (*arrow*, *D*) and also the background changes of chronic liver disease, providing a more comprehensive assessment and staging of the patient's disease process. Note the marked hypertrophy of the caudate lobe (*arrowheads*, *C* and *D*), a well-known feature of PSC.

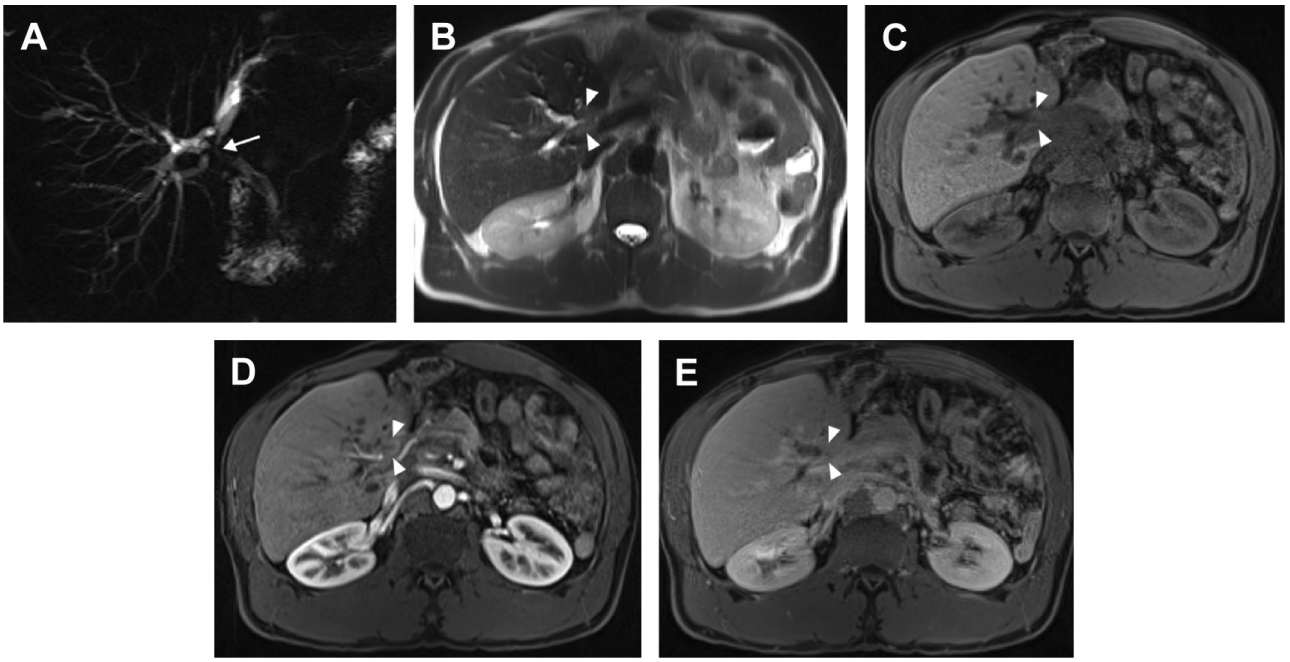

Fig. 14. A 52-year-old man with PSC and cholangiocarcinoma. Coronal slab MRCP (*A*) shows obstruction of the intrahepatic bile ducts at the confluence (*arrow*). Coronal single-shot T2W image (*B*) demonstrates infiltrative soft tissue at the site of obstruction (*arrowheads*). Axial precontrast (*C*), arterial (*D*), and delayed (*E*) postcontrast images demonstrate progressive enhancement of this soft tissue (*arrowheads*, *C–E*) in keeping with a superficial spreading cholangiocarcinoma developing in a background of PSC.

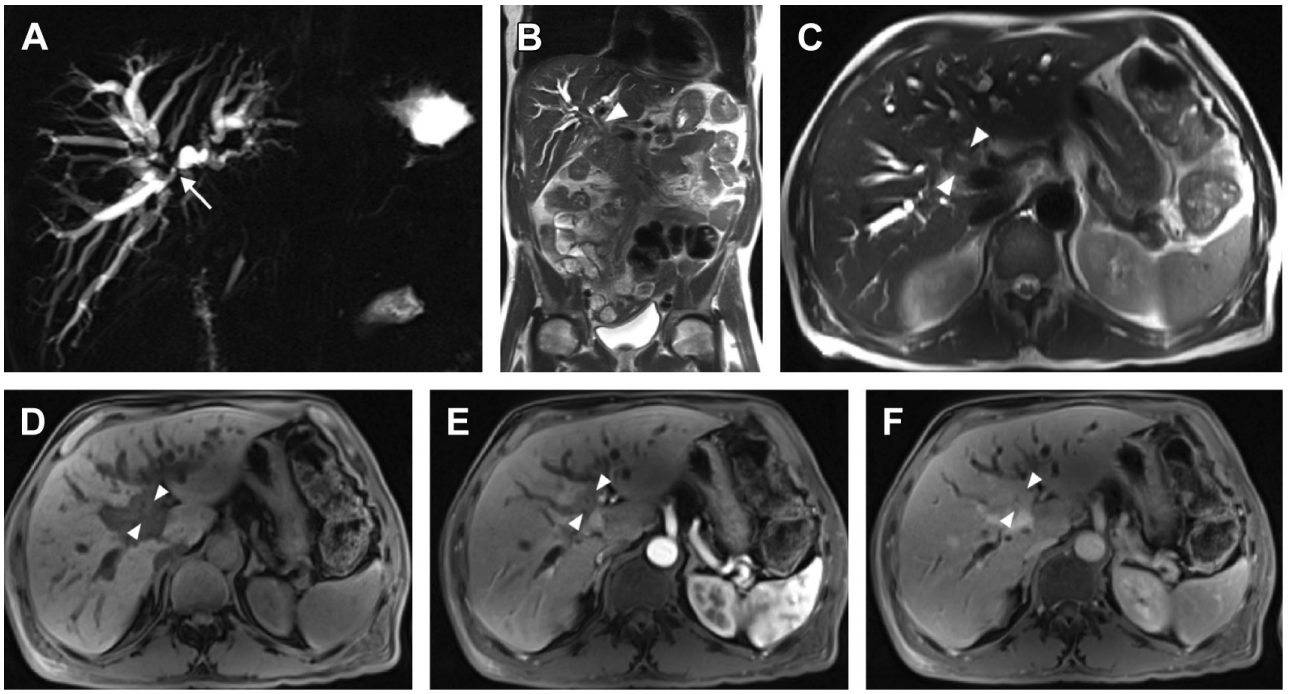

Fig. 15. A 57-year-old man with history of autoimmune pancreatitis and jaundice, pre-ERCP evaluation. Coronal slab MRCP (*A*) demonstrates biliary obstruction (*arrow*) at the level of the confluence. Coronal (*B*) and axial (*C*) single-shot T2W images depict infiltrative soft tissue growing along the biliary confluence and CHD (*arrowheads*, *B* and *C*). Axial precontrast (*D*), arterial (*E*), and delayed (*F*) phase postcontrast images shows progressive enhancement of this infiltrative soft tissue (*arrowheads*). Although these features mimic that of superficial spreading cholangiocarcinoma, the infiltrative soft tissue narrows but does not completely occlude the biliary confluence and CHD (*arrowheads*, *B*); this is a potential differentiating feature from cholangiocarcinoma.

Primary biliary cirrhosis

Primary biliary cirrhosis represents an immune-mediated disease with antimitochondrial antibodies that progressively destroys the small and middle sized intrahepatic bile ducts. This process leads initially to portal and periportal inflammation, followed by accumulating fibrous tissue and the eventual culmination in end-stage liver disease. Diagnostic imaging, including MR imaging, is not the primary method of diagnosis, but rather is part of a diagnostic algorithm including a combination of clinical, biochemical, and histopathologic assessment.[38] Frequently, many patients with documented primary biliary cirrhosis have normal imaging. When abnormalities are detected, the most common reported finding is a thin, high signal periportal halo best demonstrated on T2W imaging, corresponding to the thin perilobular fibrotic bands and perivascular cuffing seen at histology.[38] As the periportal tissues become replaced by fibrotic tissue, this periportal halo may become hypointense on T2W imaging with delayed enhancement. The primary use of diagnostic imaging in the setting of primary biliary cirrhosis is to provide comprehensive staging of background hepatic fibrosis, to evaluate for stigmata of portal hypertension, and to detect hepatocellular carcinoma.[39]

Surgical Complications

Bile duct injury

The biliary tree demonstrates a high frequency of anatomic variation, occurring in more than 50% of all individuals.[40] MR imaging is 98% accurate in the diagnosis of anatomic variants of the biliary system, and is 95% accurate in the diagnosis of cystic duct variants.[41] A detailed understanding of bile duct anatomy helps to avoid complications during laparoscopic cholecystectomy and hepatic resections. During laparoscopic cholecystectomy, biliary complications, such as bile leakage and injury to the contralateral biliary ducts, arise in 0.5% of cases, whereas after orthotopic liver transplantation, biliary complications occur in 10% to 25% of all cases.[42] There are several anatomic variants, but those with the highest potential for surgical complication include (1) aberrant right hepatic duct connecting with the common hepatic duct or cystic duct, (2) cystic duct coursing parallel to the common hepatic duct, and (3) cystic duct inserting medially onto the common hepatic duct. The most frequently occurring anatomic variation is the insertion of the right dorsocaudal intrahepatic duct into the left hepatic duct, also known as the cross-over anomaly.[43]

T2W imaging permits for rapid evaluation of the biliary tree without the need for contrast media, and three-dimensional MRCP sequences provide high-resolution detail of bile duct anatomy for presurgical planning. Newer techniques for presurgical planning of bile ducts include the use of high-resolution T1W three-dimensional GRE sequences in combination with hepatocyte-specific agents that are excreted into the biliary tree, such as Gd-EOB-DTPA.[44] The use of hepatocyte specific agents may also be helpful after bile duct injury, providing detailed assessment of the underlying structure and function of the injured bile duct and hepatic parenchyma (**Fig. 16**).

Post liver transplant biliary complications

MR imaging represents an effective diagnostic tool in the detection of biliary complications status post orthotopic liver transplantation. Following surgery, biliary complications arise with a frequency of 11% to 30% and are often indistinguishable from organ rejection, infection, or hepatic artery occlusion. Biliary complications of transplantation include bile leak, anastomotic stricture, recurrent disease (ie, cholangiocarcinoma, PSC), and cholangitis.[45] ERCP is typically not possible given altered postsurgical anatomy, and MR imaging is the imaging method of choice in this patient population.

A mucocele of the cystic duct remnant of the allograft liver represents an additional biliary complication that can lead to biliary obstruction and decreased graft organ survival. Cystic duct mucoceles occur when the opening of the cystic duct remnant of the graft liver is sewn into the biliary anastomosis, progressively distending over time and possibly obstructing the anastomosis. Cystic duct mucoceles occur in 2% to 5% of cases following transplantation, and are well depicted on MR imaging as a tubular, fluid-filled structure adjacent to the bile duct anastomosis (**Fig. 17**). Treatment involves operative resection with Roux-en-Y heapticojejunostomy.[46]

MALIGNANT HEPATOBILIARY PATHOLOGY

Cholangiocarcinoma

Cholangiocarcinoma is the most common malignancy of the biliary system. There are multiple associated risk factors, including ulcerative colitis, PSC, choledochal cysts, α_1-antitrypsin deficiency, autosomal-dominant adult polycystic kidney disease, and recurrent pyogenic cholangitis. Although there are several pathologic subtypes of cholangiocarcinoma, more than two-thirds of these tumors are of the well-differentiated, sclerosing adenocarcinoma subtype.[27] Cholangiocarcinomas are typically categorized based on their anatomic location: hilar (45%), extrahepatic (45%), and intrahepatic (10%).[47] The anatomic distribution of the

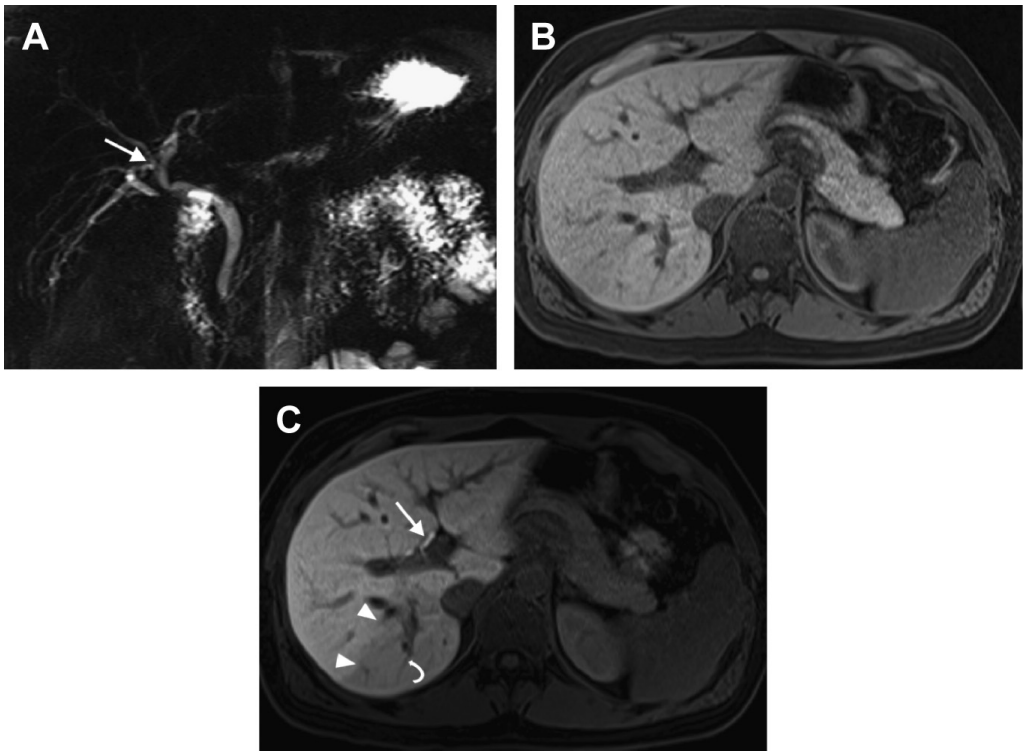

Fig. 16. A 41-year-old woman with bile duct injury status post cholecystectomy. Coronal slab MRCP (*A*) demonstrates an aberrant posterior right hepatic duct, a common predisposition to iatrogenic injury, with a focal stricture (*arrow*). Axial precontrast (*B*) and 20-minute delayed postcontrast T1W three-dimensional GRE sequences after administration of Gd-EOB-DTPA demonstrate normal excretion of the hepatocyte-specific agent into the normal left hepatic ducts (*C*, *arrow*). The obstructed posterior right hepatic duct remains unopacified with contrast (*C*, *curved arrow*), whereas the adjacent hepatic parenchyma is unable to adequately take up the contrast because of hepatocyte dysfunction from the bile duct injury (*C*, *arrowheads*). This type of functional analysis of the hepatocytes after bile duct injury is a potential advantage for the use of hepatocyte-specific gadolinium chelates in this clinical scenario.

tumor dictates the pattern of observed ductal distention and obstruction.

Hilar cholangiocarcinomas (termed Klatskin tumors) are low-volume tumors that arise at or near the confluence of the right and left hepatic ducts. Although these lesions are small, biliary obstruction is an early feature of this tumor with early presentation of clinical symptoms. Klatskin tumors grow in a superficial spreading pattern, possibly extending into the liver as the mass insinuates along the portal tracks. Given this pattern of growth and low tumor volume, these neoplasms may be difficult to diagnosis, and the soft tissue resolution of MR imaging is optimum for detection and staging of tumor. MRCP sequences are excellent for depicting the degree and level of bile duct obstruction. The identification of infiltrative soft tissue growing along and obstructing the biliary confluence is critical for diagnosis, and is readily apparent even with low-volume disease. This soft tissue is best depicted with fat-suppressed, dynamic contrast-enhanced T1W three-dimensional GRE sequences, demonstrating a progressive, delayed pattern of enhancement. The need to assess dynamic enhancement is a potential drawback for the routine use of hepatocyte-specific contrast agents in tumor diagnosis and staging. The altered biodistribution and excretion of these agents confounds the ability to evaluate dynamic enhancement patterns, a key feature for the diagnosis of cholangiocarcinoma. Single-shot T2W images without fat suppression show infiltration of the normal perihilar fat by ill-defined, hypointense T2 signal, indicative of the fibrotic nature of this tumor (**Fig. 18**). Presurgical planning involves assessment of vascular involvement and depiction of tumor extent along the portal tracks, best demonstrated on MR imaging.[27,36,44,47] Although ERCP may be performed on these patients for therapeutic biliary drainage, there is little added diagnostic benefit when compared with MR imaging. In some cases, ERCP may not be able to assess bile ducts past a point of high-grade stricture. In addition, brushings from the procedure are extremely low yield, with sensitivities of 10% to 40%,[48–51] and may potentially delay appropriate therapy in patients with disease that has already been diagnosed and staged by MR imaging (**Fig. 19**).

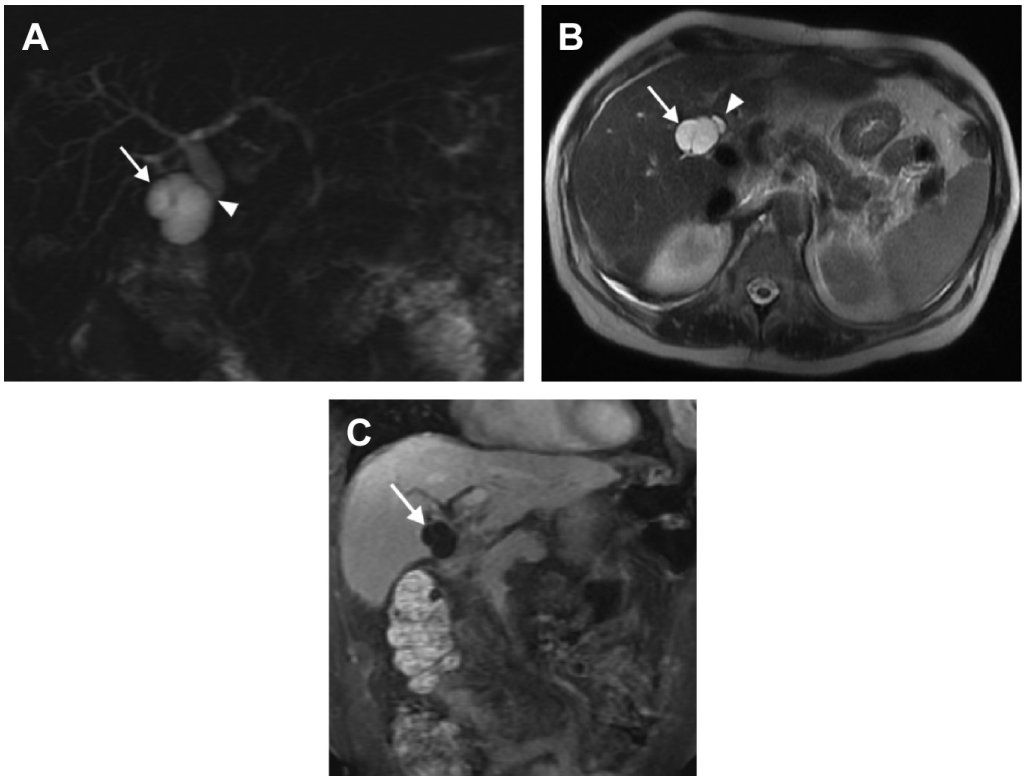

Fig. 17. A 57-year-old woman status post liver transplant with progressive dysfunction of the graft liver. (*A*) Coronal slab MRCP demonstrates dilatation of the intrahepatic and extrahepatic bile ducts with narrowing of the extrahepatic bile duct (*arrowhead*) near the anastomosis by a tubular cystic structure (*arrow*). (*B*) Axial single-shot T2W image again depicts compression of the extrahepatic bile duct (*arrowhead*) by this dilated cystic structure (*arrow*); the tubular morphology is in keeping with a distended cystic duct remnant. (*C*) Coronal postcontrast T1W three-dimensional GRE image shows no enhancement in this lesion (*arrow*) to suggest a neoplastic etiology. The patient underwent surgery with resection of the cystic duct remnant mucocele and conversion to a biliary-enteric anastomosis.

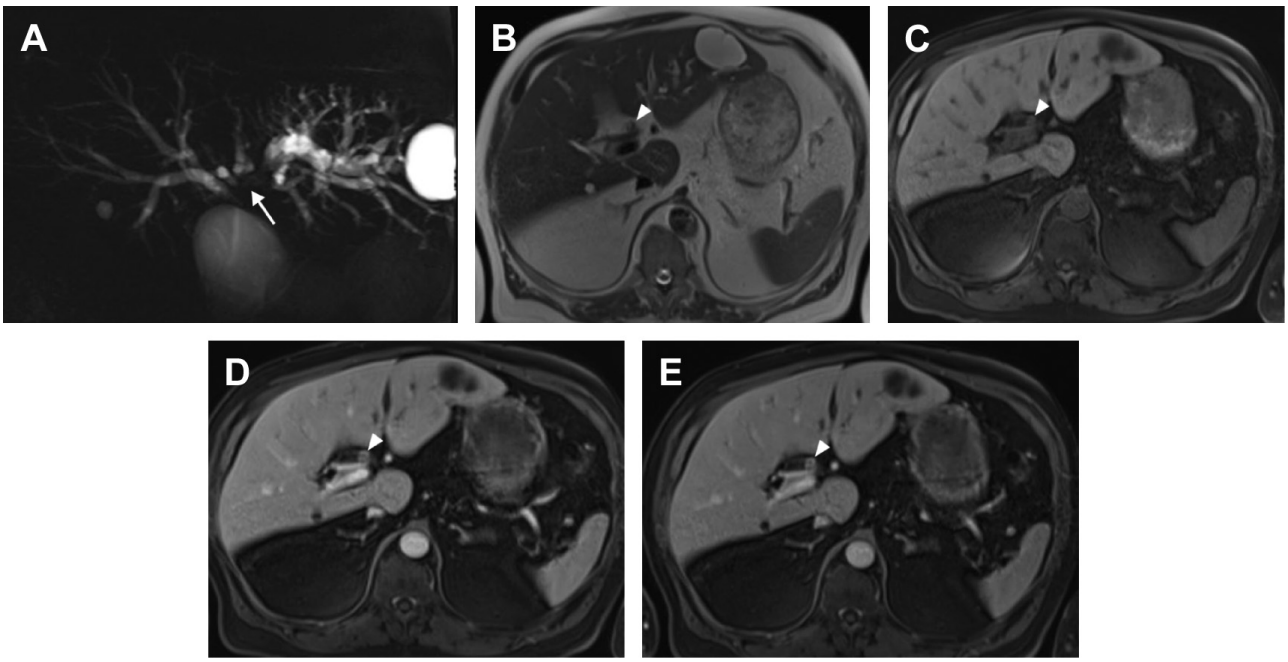

Fig. 18. A 69-year-old man with superficial spreading cholangiocarcinoma. (*A*) Coronal slab MRCP demonstrates marked intrahepatic bile duct dilatation with obstruction at the biliary confluence (*arrow*). (*B*) Axial single-shot T2W image demonstrates a thin rim of T2 hypointense tissue encircling the CHD (*arrowhead*). Axial precontrast (*C*), arterial (*D*), and delayed (*E*) phase postcontrast images demonstrate progressive enhancement of this infiltrative soft tissue (*arrowheads*, *C–E*) in keeping with superficial spreading cholangiocarcinoma, confirmed by subsequent surgical resection.

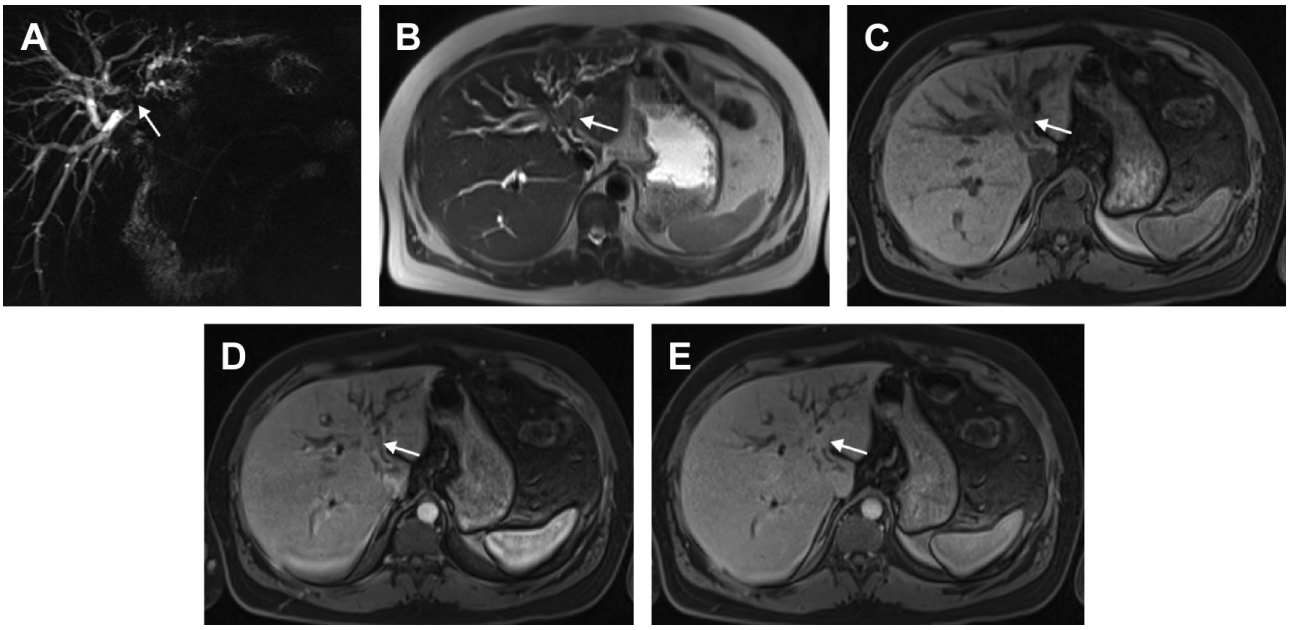

Fig. 19. A 32-year-old man with jaundice. (*A*) Coronal slab MRCP demonstrates marked intrahepatic bile duct dilatation with obstruction at the biliary confluence (*arrow*). (*B*) Axial single-shot T2W image shows infiltrative soft tissue at the site of obstruction at the hilum (*arrow*), growing preferentially along the left portal tracks. Axial precontrast (*C*), arterial (*D*), and delayed (*E*) phase postcontrast images shows progressive enhancement of this soft tissue (*arrow*) in keeping with a superficial spreading cholangiocarcinoma. This patient underwent multiple ERCPs with brushings, all negative for tumor. A second opinion at an outside medical center yielded additional ERCPs and a laparoscopic lymph node biopsy, all again negative for carcinoma. The patient returned to our center and underwent extended left hepatectomy, which confirmed the diagnosis of superficial spreading cholangiocarcinoma as depicted on the initial MR imaging.

Extrahepatic cholangiocarcinoma (EHC) also culminates in early biliary obstruction, similar to Klatskin tumors. EHC may have varying presentations, including mild irregularity of the duct at the site of obstruction, a focal mass with abrupt stricture or "shouldering" of the involved common duct, and also (less commonly) an intraluminal papillary growth pattern. Regardless of the growth pattern, EHC shows similar MR imaging features to hilar cholangiocarcinoma, with heterogeneous, delayed enhancement of the tumor on dynamic, contrast-enhanced images and hypointense T2 signal (**Fig. 20**). Note that stent placement frequently results in inflammation of the bile duct wall, causing subsequent delayed enhancement that may mimic or obscure underlying superficial spread of tumor. This reality underscores the importance of performing MR imaging before any endoscopic procedure and stent placement.

Intrahepatic cholangiocarcinoma (IHC) is a distinct neoplasm compared with the superficial spreading pattern of growth seen in hilar and EHC. IHC arises more peripherally in the hepatic parenchyma and is relatively well-encapsulated compared with other types of cholangiocarcinoma. These tumors can grow to a large size before clinical symptoms emerge or metastases occur. On MR imaging, IHC demonstrates a heterogeneous pattern of delayed enhancement on dynamic, postcontrast images. T2 signal is frequently mixed, with some areas of hypointense signal related to the fibrotic nature of the tumor. In distinction from hepatocellular carcinoma, IHC surrounds and narrows the adjacent vascular structures, which may become obliterated and collateralized. Tumor diagnosis, staging, and presurgical planning are all easily performed with MR imaging (**Fig. 21**).

Lymphoma

Diffuse B-cell lymphoma represents the most common form of lymphoma involving the biliary tree. Tumor usually involves either the common bile duct or the common hepatic duct and presents with bile duct narrowing but not necessarily with frank obstruction, a distinguishing feature from superficial spreading cholangiocarcinoma. Lymphoma may also spread along the portal tracks into the liver, causing a homogeneous pattern of progressive delayed enhancement on dynamic, contrast-enhanced imaging. T2 signal is also moderately elevated (similar to lymphatic tissue) (**Fig. 22**), and is higher signal than typically demonstrated by cholangiocarcinoma with its significant fibrotic component. Tissue sampling is typically required in these patients to confirm the diagnosis and to guide therapy.[52]

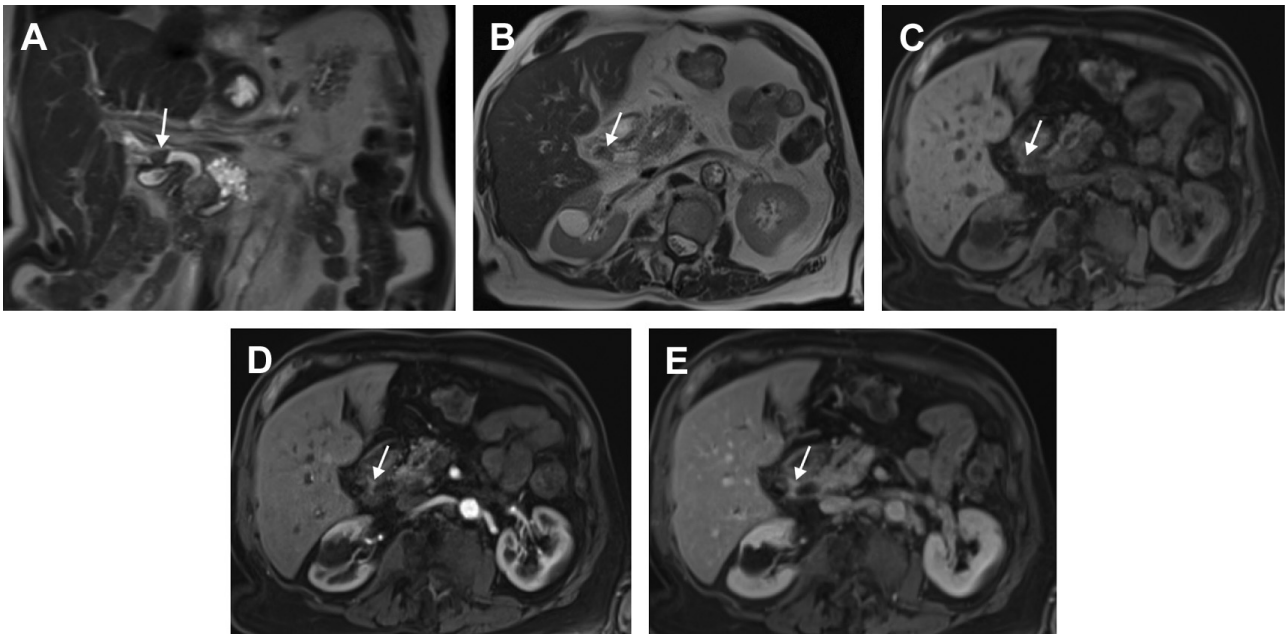

Fig. 20. A 72-year-old woman with jaundice. Coronal (*A*) and axial (*B*) single-shot T2W images show T2 hypointense soft tissue infiltrating the mid-CBD (*arrows*). Axial precontrast (*C*), arterial (*D*), and delayed (*E*) phase postcontrast sequences show progressive enhancement of this soft tissue (*arrows*) in keeping with extrahepatic cholangiocarcinoma.

Metastatic Disease

Intraepithelial spread of malignant disease along the biliary tree may be easily confused with primary malignancy of the bile ducts. Both disease processes can result in biliary obstruction and present with similar patterns of heterogeneous, delayed enhancement. Adenocarcinomas of the colon and pancreas represent the most frequently occurring metastatic processes along the bile ducts.[53]

Intraductal Papillary Neoplasms of the Bile Duct

Both the biliary and pancreatic ductal systems originate from the ventral endoderm of the foregut and may give rise to intraductal papillary

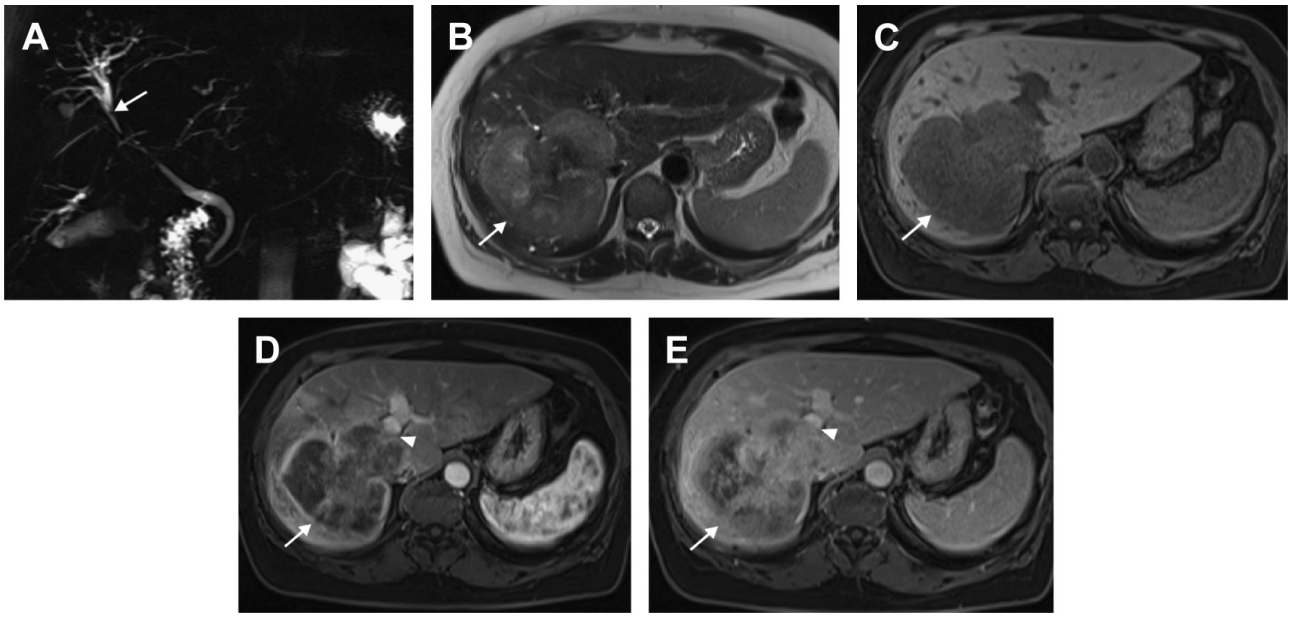

Fig. 21. A 64-year-old woman with intrahepatic cholangiocarcinoma. (*A*) Coronal slab MRCP demonstrates obstruction of the right intrahepatic bile ducts near the hilum (*arrow*). (*B*) Axial single-shot T2W image shows a large, well-circumscribed hepatic tumor with heterogeneous signal (*arrow*). Axial precontrast (*C*), arterial (*D*), and delayed (*E*) phase postcontrast images demonstrate heterogeneous, delayed enhancement (*arrows*) features in keeping with adenocarcinoma. The associated duct obstruction and portal vein occlusion (*arrowheads, D* and *E*) are typical of intrahepatic cholangiocarcinoma.

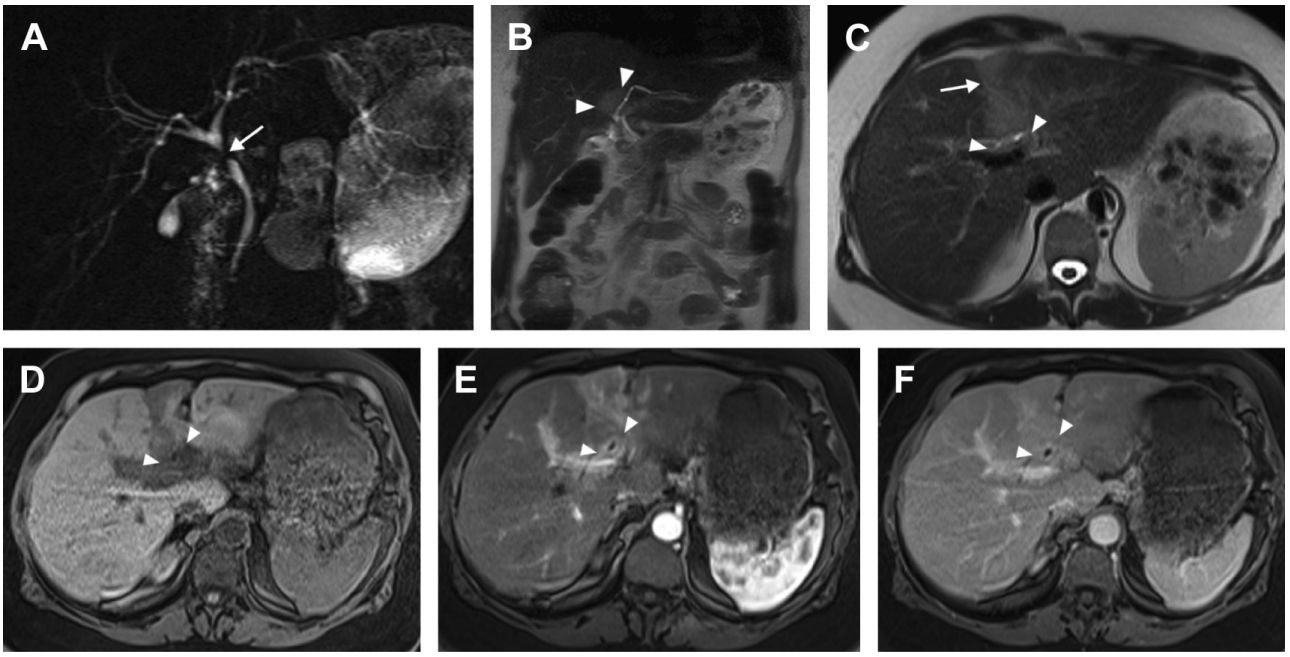

Fig. 22. A 50-year-old woman with jaundice. (*A*) Coronal slab MRCP demonstrates smooth stenosis (*arrow*) of the CHD with mild intrahepatic bile duct dilatation. Coronal (*B*) and axial (*C*) single-shot T2W images demonstrate infiltrative, mildly hyperintense soft tissue surrounding the biliary confluence (*arrowheads*, *B* and *C*) and tracking into the left hepatic lobe (*arrow*, *C*). Note this infiltrative tissue demonstrates T2 signal similar to lymphoid tissue. Axial precontrast (*D*), arterial (*E*), and delayed (*F*) phase postcontrast sequences demonstrate homogeneous delayed enhancement of this tissue (*arrowheads*) that surrounds and narrows the biliary confluence without high-grade obstruction. These features are consistent with lymphomatous infiltration, which was confirmed with tissue sampling.

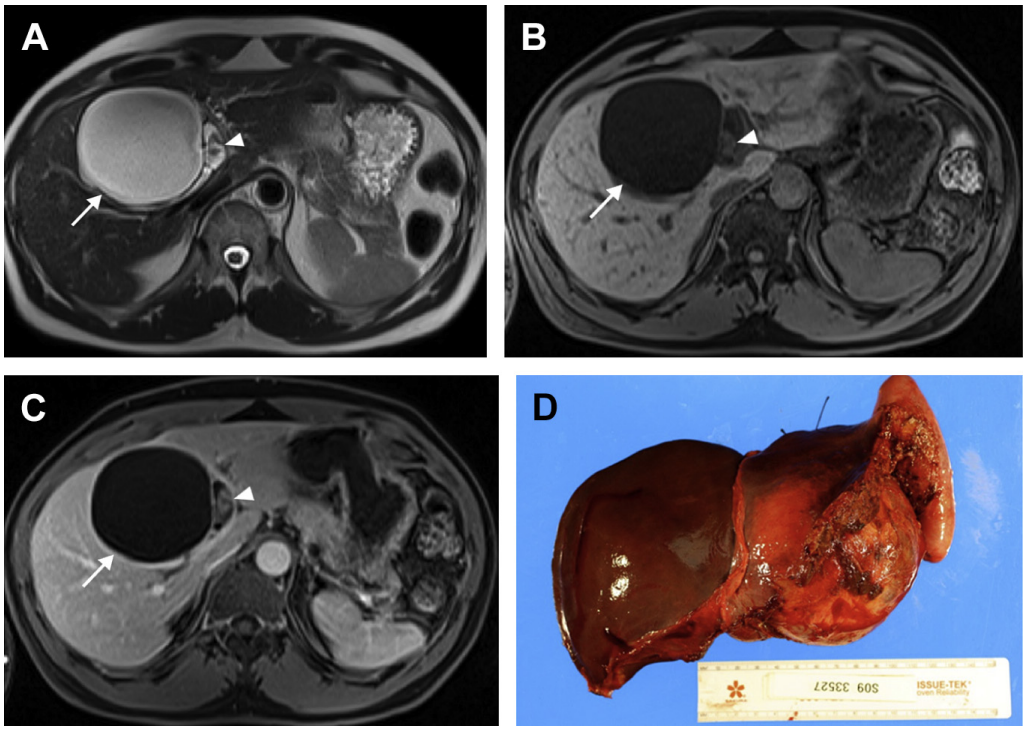

Fig. 23. A 56-year-old man with intraductal papillary neoplasm of the bile duct. (*A*) Axial single-shot T2W image depicts a large, complex cystic lesion in the liver (*arrow*) with a small focus of soft tissue along the medial margin (*arrowhead*). Communication with the biliary system was identified on MRCP sequences (not shown). Axial precontrast (*B*) and postcontrast (*C*) images demonstrate enhancement of the soft tissue nodule along the medial margin (*arrowheads*, *B* and *C*) of the cystic tumor (*arrows*), consistent with carcinomatous elements. (*D*) Gross surgical specimen shows the large cystic tumor along the undersurface of the left hepatic lobe, confirmed on histolopathologic analysis to be an intraductal papillary neoplasm of the bile ducts with associated carcinoma.

neoplasms (IPN). IPN of the bile duct consists of intraluminal papillary tumors with fibrovasular cores that produce an excess of mucin and distend the bile duct with a tubular, fusiform, or cystic morphology. In contrast to intraductal papillary mucinous neoplasm (IPMN) of the pancreas, IPN of the bile duct develop as carcinoma in situ. IPN of the biliary system lacks ovarian stroma within its wall, clearly differentiating it from a biliary cystadenoma. In addition, IPN of the bile duct demonstrates a luminal communication with the bile duct via a diverticulum arising from a peribiliary gland, in contrast to a biliary cystadenoma, which fails to demonstrate communication with the biliary system.[54,55] On MR imaging, bile duct IPN presents as rounded or tubular cystic lesions with associated ductal communication that is best depicted on T2W images. Postcontrast images are critical to assess for coexistent carcinomatous elements (**Fig. 23**), which are present in most cases.

SUMMARY

MR imaging represents an excellent noninvasive imaging technique for the evaluation of the biliary system. In the diagnosis of benign biliary disease, MR imaging demonstrates diagnostic accuracy comparable with ERCP but without the associated morbidity, whereas malignant diseases are more fully staged with MR imaging. Although two- and three-dimensional MRCP techniques provide excellent depiction of the bile ducts, dynamic contrast-enhanced T1W three-dimensional GRE sequences are critical to provide a comprehensive evaluation of biliary pathology. Novel hepatocyte-specific contrast agents are now available that have the potential to provide additional information regarding anatomy and function of the bile ducts.

REFERENCES

1. Fulcher AS, Turner MA, Capps GW. MR cholangiography: technical advances and clinical applications. Radiographics 1999;19(1):25–41 [discussion: 41–4].
2. Fulcher AS, Turner MA, Capps GW, et al. Half-Fourier RARE MR cholangiopancreatography: experience in 300 subjects. Radiology 1998;207(1):21–32.
3. Hosseinzadeh K, Furlan A, Almusa O. 2D thick-slab MR cholangiopancreatography: does parallel imaging with sensitivity encoding improve image quality and duct visualization? AJR Am J Roentgenol 2008;190(6):W327–34.
4. Zhang J, Israel GM, Hecht EM, et al. Isotropic 3D T2-weighted MR cholangiopancreatography with parallel imaging: feasibility study. AJR Am J Roentgenol 2006;187(6):1564–70.
5. Soto JA, Barish MA, Alvarez O, et al. Detection of choledocholithiasis with MR cholangiography: comparison of three-dimensional fast spin-echo and single- and multisection half-Fourier rapid acquisition with relaxation enhancement sequences. Radiology 2000;215(3):737–45.
6. Hiraishi K, Sagami A, Hisada Y, et al. Contrast enhancement effect of new oral agent (blueberry juice) for upper abdominal MR imaging. Nihon Igaku Hoshasen Gakkai Zasshi 1994;54(6):539–41 [in Japanese].
7. Chandarana H, Block TK, Rosenkrantz AB, et al. Free-breathing radial 3D fat-suppressed T1-weighted gradient echo sequence: a viable alternative for contrast-enhanced liver imaging in patients unable to suspend respiration. Invest Radiol 2011;46(10):648–53.
8. Braren R, Curcic J, Remmele S, et al. Free-breathing quantitative dynamic contrast-enhanced magnetic resonance imaging in a rat liver tumor model using dynamic radial T(1) mapping. Invest Radiol 2011;46(10):624–31.
9. Allen K, Jaeschke H, Copple BL. Bile acids induce inflammatory genes in hepatocytes: a novel mechanism of inflammation during obstructive cholestasis. Am J Pathol 2011;178(1):175–86.
10. Sharma P, Kalb B, Kitajima HD, et al. Optimization of single injection liver arterial phase gadolinium enhanced MRI using bolus track real-time imaging. J Magn Reson Imaging 2011;33(1):110–8.
11. Yam BL, Siegelman ES. MR imaging of the biliary system. Radiol Clin North Am 2014;52(4):725–55.
12. Jia J, Puls D, Oswald S, et al. Characterization of the intestinal and hepatic uptake/efflux transport of the magnetic resonance imaging contrast agent gadolinium-ethoxylbenzyl-diethylenetriamine-pentaacetic acid. Invest Radiol 2014;49(2):78–86.
13. Nagle SK, Busse RF, Brau AC, et al. High resolution navigated three-dimensional T(1)-weighted hepatobiliary MRI using gadoxetic acid optimized for 1.5 Tesla. J Magn Reson Imaging 2012;36(4):890–9.
14. Andriulli A, Loperfido S, Napolitano G, et al. Incidence rates of post-ERCP complications: a systematic survey of prospective studies. Am J Gastroenterol 2007;102(8):1781–8.
15. Christensen M, Matzen P, Schulze S, et al. Complications of ERCP: a prospective study. Gastrointest Endosc 2004;60(5):721–31.
16. Park DH, Kim MH, Lee SK, et al. Can MRCP replace the diagnostic role of ERCP for patients with choledochal cysts? Gastrointest Endosc 2005;62(3):360–6.
17. Park MS, Kim TK, Kim KW, et al. Differentiation of extrahepatic bile duct cholangiocarcinoma from benign stricture: findings at MRCP versus ERCP. Radiology 2004;233(1):234–40.

18. Park HS, Lee JM, Choi JY, et al. Preoperative evaluation of bile duct cancer: MRI combined with MR cholangiopancreatography versus MDCT with direct cholangiography. AJR Am J Roentgenol 2008;190(2):396–405.
19. Chapman R, Fevery J, Kalloo A, et al. Diagnosis and management of primary sclerosing cholangitis. Hepatology 2010;51(2):660–78.
20. Vergel YB, Chilcott J, Kaltenthaler E, et al. Economic evaluation of MR cholangiopancreatography compared to diagnostic ERCP for the investigation of biliary tree obstruction. Int J Surg 2006;4(1):12–9.
21. Turner MA, Fulcher AS. The cystic duct: normal anatomy and disease processes. Radiographics 2001;21(1):3–22.
22. Besa C, Cruz JP, Huete A, et al. Portal biliopathy: a multitechnique imaging approach. Abdom Imaging 2012;37(1):83–90.
23. Song B, Min P, Oudkerk M, et al. Cavernous transformation of the portal vein secondary to tumor thrombosis of hepatocellular carcinoma: spiral CT visualization of the collateral vessels. Abdom Imaging 2000;25(4):385–93.
24. Todani T, Watanabe Y, Narusue M, et al. Congenital bile duct cysts: classification, operative procedures, and review of thirty-seven cases including cancer arising from choledochal cyst. Am J Surg 1977;134(2):263–9.
25. Govil S, Justus A, Korah I, et al. Choledochal cysts: evaluation with MR cholangiography. Abdom Imaging 1998;23(6):616–9.
26. Flanigan DP. Biliary carcinoma associated with biliary cysts. Cancer 1977;40(2):880–3.
27. Bilgin M, Shaikh F, Semelka RC, et al. Magnetic resonance imaging of gallbladder and biliary system. Top Magn Reson Imaging 2009;20(1):31–42.
28. Ohashi T, Wakai T, Kubota M, et al. Risk of subsequent biliary malignancy in patients undergoing cyst excision for congenital choledochal cysts. J Gastroenterol Hepatol 2013;28(2):243–7.
29. Martin DR, Seibert D, Yang M, et al. Reversible heterogeneous arterial phase liver perfusion associated with transient acute hepatitis: findings on gadolinium-enhanced MRI. J Magn Reson Imaging 2004;20(5):838–42.
30. Eun HW, Kim JH, Hong SS, et al. Assessment of acute cholangitis by MR imaging. Eur J Radiol 2012;81(10):2476–80.
31. Garcia-Gutierrez M, Luque-Marquez R, Rodriguez-Suarez S. Portal vein thrombosis associated with biliary tract infection. Gastroenterol Hepatol 2012; 35(9):644–8 [in Spanish].
32. Park MS, Yu JS, Kim KW, et al. Recurrent pyogenic cholangitis: comparison between MR cholangiography and direct cholangiography. Radiology 2001;220(3):677–82.
33. Heffernan EJ, Geoghegan T, Munk PL, et al. Recurrent pyogenic cholangitis: from imaging to intervention. AJR Am J Roentgenol 2009;192(1):W28–35.
34. Mendes F, Lindor KD. Primary sclerosing cholangitis: overview and update. Nat Rev Gastroenterol Hepatol 2010;7(11):611–9.
35. Garg D, Nagar A, Philips S, et al. Immunological diseases of the pancreatico-hepatobiliary system: update on etiopathogenesis and cross-sectional imaging findings. Abdom Imaging 2012;37(2): 261–74.
36. Bilgin M, Balci NC, Erdogan A, et al. Hepatobiliary and pancreatic MRI and MRCP findings in patients with HIV infection. AJR Am J Roentgenol 2008; 191(1):228–32.
37. Wilcox CM, Monkemuller KE. Hepatobiliary diseases in patients with AIDS: focus on AIDS cholangiopathy and gallbladder disease. Dig Dis 1998; 16(4):205–13.
38. Nguyen DL, Juran BD, Lazaridis KN. Primary biliary cirrhosis. Best Pract Res Clin Gastroenterol 2010; 24(5):647–54.
39. Kovac JD, Jesic R, Stanisavljevic D, et al. Integrative role of MRI in the evaluation of primary biliary cirrhosis. Eur Radiol 2012;22(3):688–94.
40. Northover J, Terblanche J. Applied surgical anatomy of the biliary tree. Clin Surg Int 1982;5:1–16.
41. Taourel P, Bret PM, Reinhold C, et al. Anatomic variants of the biliary tree: diagnosis with MR cholangiopancreatography. Radiology 1996;199(2): 521–7.
42. Kapoor V, Baron RL, Peterson MS. Bile leaks after surgery. AJR Am J Roentgenol 2004;182(2): 451–8.
43. Hirao K, Miyazaki A, Fujimoto T, et al. Evaluation of aberrant bile ducts before laparoscopic cholecystectomy: helical CT cholangiography versus MR cholangiography. AJR Am J Roentgenol 2000; 175(3):713–20.
44. Frydrychowicz A, Lubner MG, Brown JJ, et al. Hepatobiliary MR imaging with gadolinium-based contrast agents. J Magn Reson Imaging 2012; 35(3):492–511.
45. Itri JN, Heller MT, Tublin ME. Hepatic transplantation: postoperative complications. Abdom Imaging 2013;38:1300–33.
46. Chatterjee S, Das D, Hudson M, et al. Mucocele of the cystic duct remnant after orthotopic liver transplant: a problem revisited. Exp Clin Transplant 2011;9(3):214–6.
47. Hamrick-Turner J, Abbitt PL, Ros PR. Intrahepatic cholangiocarcinoma: MR appearance. AJR Am J Roentgenol 1992;158(1):77–9.
48. Hekimoglu K, Ustundag Y, Dusak A, et al. MRCP vs. ERCP in the evaluation of biliary pathologies: review of current literature. J Dig Dis 2008;9(3): 162–9.

49. Hyodo T, Kumano S, Kushihata F, et al. CT and MR cholangiography: advantages and pitfalls in perioperative evaluation of biliary tree. Br J Radiol 2012;85(1015):887–96.
50. Lee DH, Lee JM, Kim KW, et al. MR imaging findings of early bile duct cancer. J Magn Reson Imaging 2008;28(6):1466–75.
51. Masui T, Katayama M, Kobayashi S, et al. Magnetic resonance cholangiopancreatography: comparison of respiratory-triggered three-dimensional fast-recovery fast spin-echo with parallel imaging technique and breath-hold half-Fourier two-dimensional single-shot fast spin-echo technique. Radiat Med 2006;24(3):202–9.
52. Ghose A, Sethi N, Li G, et al. Chemotherapy versus surgery in primary B-cell lymphoma masquerading as Klatskin tumor: a diagnostic and therapeutic dilemma. Am J Ther 2011;18(6):e255–7.
53. Riopel MA, Klimstra DS, Godellas CV, et al. Intrabiliary growth of metastatic colonic adenocarcinoma: a pattern of intrahepatic spread easily confused with primary neoplasia of the biliary tract. Am J Surg Pathol 1997;21(9):1030–6.
54. Lim JH, Zen Y, Jang KT, et al. Cyst-forming intraductal papillary neoplasm of the bile ducts: description of imaging and pathologic aspects. AJR Am J Roentgenol 2011;197(5):1111–20.
55. Bosman FT, Carneiro F, Hurban RH, et al. WHO classification of tumours of digestive system. Lyon (France): International Agency for Research on Cancer Press; 2010.